MIT

FINITE ELEMENT ANALYSIS OF ELASTO-PLASTIC SOILS

by

W. Allen Marr, Jr.

John T. Christian

Report No. 4
Finite Element Analysis of Elasto-Plastic
Frictional Materials for Application to
Lunar Earth Sciences

Contract No. NASA-9990
Soils Publication No. 301
Research Report R72-21

June 1972

Sponsored by
National Aeronautics and Space Administration
Manned Spacecraft Center
Houston, Texas

DEPARTMENT
OF
CIVIL
ENGINEERING

SCHOOL OF ENGINEERING
MASSACHUSETTS INSTITUTE OF TECHNOLOGY
Cambridge, Massachusetts 02139

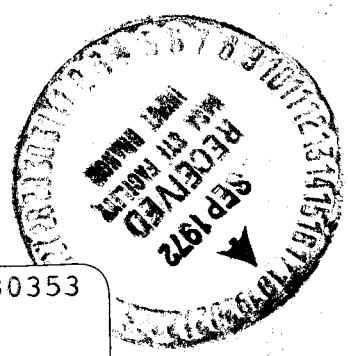

FINITE ELEMENT ANALYSIS OF ELASTO-PLASTIC SOILS

by
WILLIAM ALLEN MARR, JR.
JOHN T. CHRISTIAN

Report No. 4
Contract No. NASA-9990
Finite Element Analysis of Elasto-Plastic Frictional Materials for Application to Lunar Earth Sciences

Sponsored by
National Aeronautics and Space Administration
Manned Spacecraft Center
Houston, Texas

Soil Mechanics Division
Department of Civil Engineering
Massachusetts Institute of Technology
Cambridge, Massachusetts

April 1972

Soils Publication No. 301
Research Report R72-21

/

ABSTRACT

FINITE ELEMENT ANALYSIS OF ELASTO-PLASTIC SOILS

Predictions of the stresses and displacements in soil masses resulting from changes in load are important in the design and construction of many civil engineering structures. Such predictions require the use of an appropriate constitutive relation which defines the stress-strain behavior of soil.

The behavior of finite element models employing different constitutive relations to describe the stress-strain behavior of soils is investigated. Three models, which assume small strain theory is applicable, include a non-dilatant, a dilatant and a strain hardening constitutive relation. Two models are formulated using large strain theory and include a hyperbolic and a Tresca elastic perfectly plastic constitutive relation.

These finite element models are used to analyze retaining walls and footings. Excellent solutions are obtained for the failure load of retaining walls in drained frictional material. Attempts to obtain the failure load of footings in drained frictional materials are only moderately successful. Good solutions are obtained for the failure of footings on purely cohesive soil using both the small strain and large strain formulations.

Methods of improving the finite element solutions are investigated. For non-linear problems better solutions can be obtained by using smaller load increment sizes and more iterations per load increment than by increasing the number of elements. Suitable methods of treating tension stresses and stresses which exceed the yield criteria are discussed.

ACKNOWLEDGMENTS

I am grateful to Professor John T. Christian, who served as my thesis supervisor, for his guidance, encouragement and personal interest in my educational development.

The assistance of Miss Sharon Niles and Mrs. Lelia de Passos in typing the manuscript and drafting the figures is greatly appreciated.

This thesis research was part of a research program sponsored by the National Aeronautics and Space Administration. I am indebted to the National Science Foundation and to Woodward-Clyde Consultants in cooperation with the Consulting Engineers Council of the U.S. for their financial support of my graduate education.

CONTENTS

TABLES

FIGURES

CHAPTER 1

INTRODUCTION

Major applications of the principles of soil mechanics involve prediction of stresses and displacements induced by changes in loading. Since the development of the discipline of soil mechanics by Karl Terzaghi (1923, 1943), researchers and practitioners have attempted to formulate and refine constitutive relations defining the stress-strain behavior of soils. Such constitutive relations are usually non-linear, and, when coupled with the complex geometry, material properties, and boundary conditions prevailing in most practical problems, they render closed form or analytical solutions impossible. Consequently, numerical procedures have been developed, that will handle these complexities. Recently the most popular and successful numerical procedure has been the finite element method because it is simple and flexible.

The object of this research is to investigate the behavior of finite element models employing different constitutive relations to describe the stress-strain behavior of soils. The behavior of these constitutive relations and their ability to solve problems for which analytical solutions are available will be presented. Methods to improve the finite element solution of these

problems will also be considered.

Five constitutive models are employed. Three models assume that small displacements result from each load application so that infinitesimal strain theory is applicable. These are a strain hardening model that is similar to the Cambridge Clay model formulated by Roscoe and his co-workers (1963, 1968) and two elasto-plastic models using a Mohr-Coulomb yield criterion. The other two models assume that appreciable changes in geometry may occur upon loading. This requires a large-strain formulation. The constitutive relations are a perfectly plastic Tresca material and a hyperbolic approximation of the experimental stress-strain curve for a given soil.

The derivations of the constitutive relations and detailed descriptions of the finite element programs are given by Hagmann (1971) and Molina (1971). Only pertinent portions will be cited in this report. Chapter 2 reviews the basic assumptions of the constitutive relations and general descriptions of the finite element programs. Chapter 3 discusses the effects of varying the finite element model and describes modifications made to the small strain programs to improve their performance. Chapter 4 compares the finite element solutions with existing solutions for bearing capacity and retaining wall problems and discusses the ability of the constitutive relations to pre-

dict stress-strain behavior of soil. Chapter 5 presents conclusions and recommendations for further study.

CHAPTER 2

DESCRIPTIONS OF CONSTITUTIVE RELATIONS AND FINITE ELEMENT PROGRAMS

The basic finite element method has been described by many authors (see Clough, 1965; Felippa, 1966; Zienkiewicz, 1971) and will not be discussed in detail in this report. The finite element model is formed by subdividing the soil medium into a finite number of discrete parts or elements interconnected at the element corners or nodes. Each element must satisfy the following requirements:

Equilibrium must exist between externally applied forces and internal stresses.

Displacements between and inside elements must be compatible.

Stresses and displacements within each element must satisfy the stress strain relationship assigned to that element.

The entire assemblage of elements must remain in equilibrium.

To satisfy these requirements, the direct stiffness or displacement method is applied (Clough, 1966). A system of simultaneous equations is obtained which relate nodal forces to nodal displacements by stiffness coefficients which are a function of element material properties and

element geometry. These equations are solved for the nodal displacements from which the element deformations, strains, and stresses may be calculated.

A two-dimensional element known as the constant strain triangle is used in all the finite element programs discussed in this report. Strain and stress are constant throughout the element; consequently, displacements vary linearly within the element. If four constant strain triangles are grouped together to form a quadrilateral, the center node displacements will depend only on the displacements of the four nodes forming the quadrilateral corners. The center node displacements can be expressed as functions of the displacements of the quadrilateral corner nodes and may be removed from the matrix of displacement unknowns, a technique known as static condensation and described by Wilson (1965). The value of stress and strain in the quadrilateral element is then taken as the average of the values for the four triangular elements. Quadrilateral elements are input to the programs, which subsequently divide each quadrilateral into four triangles to compute element stiffnesses, stresses and strains.

All programs are for plane strain conditions. Loads are applied statically and incrementally. No time effects or pore pressures are considered. The constitutive relations have been selected and computer programs have been

written to utilize physical material properties readily obtainable from standard testing techniques. With the exception of the hyperbolic constitutive relation, all programs assume that the material properties governing elastic deformations are isotropic. The hyperbolic model uses an interpolation procedure to account for anisotropic elasticity.

Each of the five constitutive relations and finite element programs is discussed below. The first three models are for small strain analysis and are described in more detail by Hagmann (1971). The remaining two are large strain formulations and are described by Molina (1971). Table 2.1 summarizes each model and the soil parameters required as input for the finite element programs.

2.1 Elasto-Plastic Dilatant Mohr-Coulomb Material

This program analyzes drained, frictional materials assuming they obey the Mohr-Coulomb failure criterion which states that the ultimate shear strength of a material is related to the normal stress on the failure plane times an angle of internal friction plus material cohesion, or

$$\tau_{ff} = c - \sigma_{ff} \tan\phi \qquad (2\text{-}1)$$

where the sign convention is tension positive. (Appendix A defines the symbols used in the text.) Figure 2-1 illustrates the failure envelope described by Eq. 2-1 in terms of p, the mean normal stress, and q, the deviatoric stress,

$$p = \frac{\sigma_1+\sigma_3}{2} = \frac{\sigma_{xx}+\sigma_{zz}}{2}$$

$$q = \frac{\sigma_1-\sigma_3}{2} = \left[\left(\frac{\sigma_{xx}-\sigma_{zz}}{2}\right)^2 + \tau_{xz}^2\right]^{\frac{1}{2}} \qquad (2\text{-}2)$$

where σ_1 and σ_3 are the major and minor principle stresses. The Mohr-Coulomb failure law assumes that the intermediate principal stress has no effect on the failure stress.

Any change in the state of stress that produces a final stress state below the Mohr-Coulomb envelope is assumed to induce elastic strains, and the constitutive relation yields the well known perfectly elastic stress-strain equations for plane strain (Timoshenko and Goodier, 1951). Once the stress state reaches the Mohr-Coulomb envelope, the element must yield. Now the constitutive equations become the perfectly plastic incremental relations developed from the theory of the plastic potential (von Mises, 1928). This theory states that the increments of plastic strain are proportional to the gradient or outward normal to the yield criterion. Hagmann et al. (1970) describe in detail the derivation of the incremental elastic-

plastic stress strain relations, one consequence of which is that there is a constant plastic volume increase during shear at the Mohr-Coulomb surface. Figure 2.2 illustrates the strains produced by this constitutive relation. Drucker and Prager (1952) and Christian (1966) describe these results of plasticity theory for frictional soils. In nature dense sands and overconsolidated clays experience volumetric increases during shear but eventually reach a state of constant volume, so there is a discrepancy between the plastic theory and experimental observation.

2.2 Elasto-Plastic Non-Dilatant Mohr-Coulomb Material

The dilatant Mohr-Coulomb model described in the previous section predicts large and continuous increases in volume during shear, a prediction that is not in accordance with observed behavior. To correct this a non-dilatant Mohr-Coulomb model was developed. It starts from the same incremental plastic strain that the dilatant model uses, but the volumetric component of the plastic strain increment is removed to give a non-dilatant plastic behavior. Hagmann et al. (1970, 1971) describe the derivation in detail. The difference between the two Mohr-Coulomb models lies only in the incremental stress-strain relations for plastic material. In the non-dilatant case this relation is unsymmetric. Figure 2.3 illustrates this constitutive

relation.

The finite element computer program and input parameters for the non-dilatant model are the same as for the dilatant model. An input code directs which plastic stress-strain relations are to be used.

2.3 Strain Hardening Mohr-Coulomb Material

The strain hardening model introduces an additional yield surface below the Mohr-Coulomb failure envelope, which allows plastic strains to occur for stress changes below the failure line. No plastic or irrecoverable strains occur below the Mohr-Coulomb failure envelope in the dilatant and non-dilatant models. However, all soils do exhibit irrecoverable strains (except some dense sands and overconsolidated clays at very low stress levels). The strain hardening model produces irrecoverable strains for stress changes on the capped yield surface.

The combination of the Mohr-Coulomb failure line with a capped yield surface which moves with changes in stress level was proposed by Drucker, Henkel, and Gibson (1957). Roscoe and his associates (1958, 1963, 1968) modified the basic capped yield criterion theory to describe better the strain behavior of clays. Christian (1966) suggested that the capped yield surface be modelled as an ellipse to simplify the mathematical relations.

Figure 2.4 illustrates the yield surface for the strain hardening model. To illustrate how this model works, consider point X in Figure 2.4 which represents the initial state of stress in an element. An increment of load is applied. If the stress path for that increment is line XY, the resulting strains will be elastic. If the stress path is line XCD, then the element will yield plastically along CD with elastic strains resulting along XC. For stress path XMN, XM will result in elastic strain and MN will cause plastic strains. In addition, the elliptical yield surface will move outward to A'NB', and during subsequent load increments all strains within A'NB' and the Mohr-Coulomb envelope will be elastic. Hagmann (1971) describes the incremental stress-strain relations for the strain hardening model.

2.4 Elastic-Perfectly Plastic Tresca Material

This model for large strains is developed from an approach described by Biot (1965) for the incremental deformation of initially stressed mediums. The derivation assumes that incremental stresses are infinitesimal with respect to initial stresses. For large strain theory, higher order terms in the stress-strain and geometrical equations become important; consequently, second order terms are included in the constitutive relations for this

model. The soil is assumed to fail according to the Tresca yield criterion which states that at some constant value of shear stress the material will yield. The soil is assumed to behave elasticly before yield and perfectly plastic once the shear stress has reached the yield value. The Tresca yield criterion is valid only for saturated undrained soils, and it is thus applicable primarily to undrained loading of clays. The details of the large strain model are described by Molina (1971).

2.5 Hyperbolic Stress-Strain Relation

The hyperbolic relation assumes that the stress-strain curve for a soil can be approximated by a hyperbola. This non-linear relationship is replaced with a series of straight lines each of which is tangent to the hyperbolic stress-strain curve at some point. Tangent moduli values, which are a function of the stress level, are computed from the hyperbolic approximation. Strains are obtained for each load increment using tangent moduli values computed from the stresses in the preceding increment and the elastic constitutive relations for plane strain.

Kondner (1963) and Kondner and Zelasko (1963) have shown that the stress-strain curves of many soils can be approximated by a hyperbola. However, many soils, including dense sands and overconsolidated clays, experience a

decrease in strength once the peak strength is reached. With the present finite element formulation it is not possible to simulate a stress-strain relationship in which the strength decreases beyond a peak. To do so requires negative modulus values and the finite element method will not converge to a solution. Consequently, when an element reaches the peak strength, modulus values are approximated by a straight line of small positive slope.

The hyperbolic stress-strain relation was first applied in finite element methods by Duncan and his coworkers (see for example Duncan and Chang (1971)). They derived the incremental or tangent form of the relationship. The extension to large strain cases was made by Molina (1971).

Table 2.1 SUMMARY OF COMPUTER PROGRAMS AND INPUT PARAMETERS

Constitutive Relation	Program Acronym	Formulation	Input Soil Parameters[1]
Elasto-Plastic Dilatant Mohr-Coulomb Material	FEAMOC	Small-strain	$E, \mu, \gamma, K_o, \phi, c$, code for dilatant constitutive relation
Elasto-Plastic Non-Dilatant Mohr-Coulomb Material	FEAMOC	Small-strain	$E, \mu, \gamma, K_o, \phi, c$, code for non-dilatant constitutive relation
Strain Hardening Mohr-Coulomb Material	FEAHAR	Small-strain	$E, \mu, \gamma, K_o, \phi, c, D, C_d, \beta$
Elastic-Perfectly Plastic Tresca Material	FELSP	Large-strain	$B, G, \mu, \gamma, K_o, c=S_u, A_f$
Hyperbolic Stress-Strain Relation	FELSH	Large-strain	$C_p, C_a, \phi, K_B, \mu, K'_p, K'_a, K_{up}, K_{ua}, R_{f_p}, R_{f_a}, n'_p, n'_a, G_{ult}, A_f, \gamma, K_o$

[1] See Appendix A for definition of symbols.

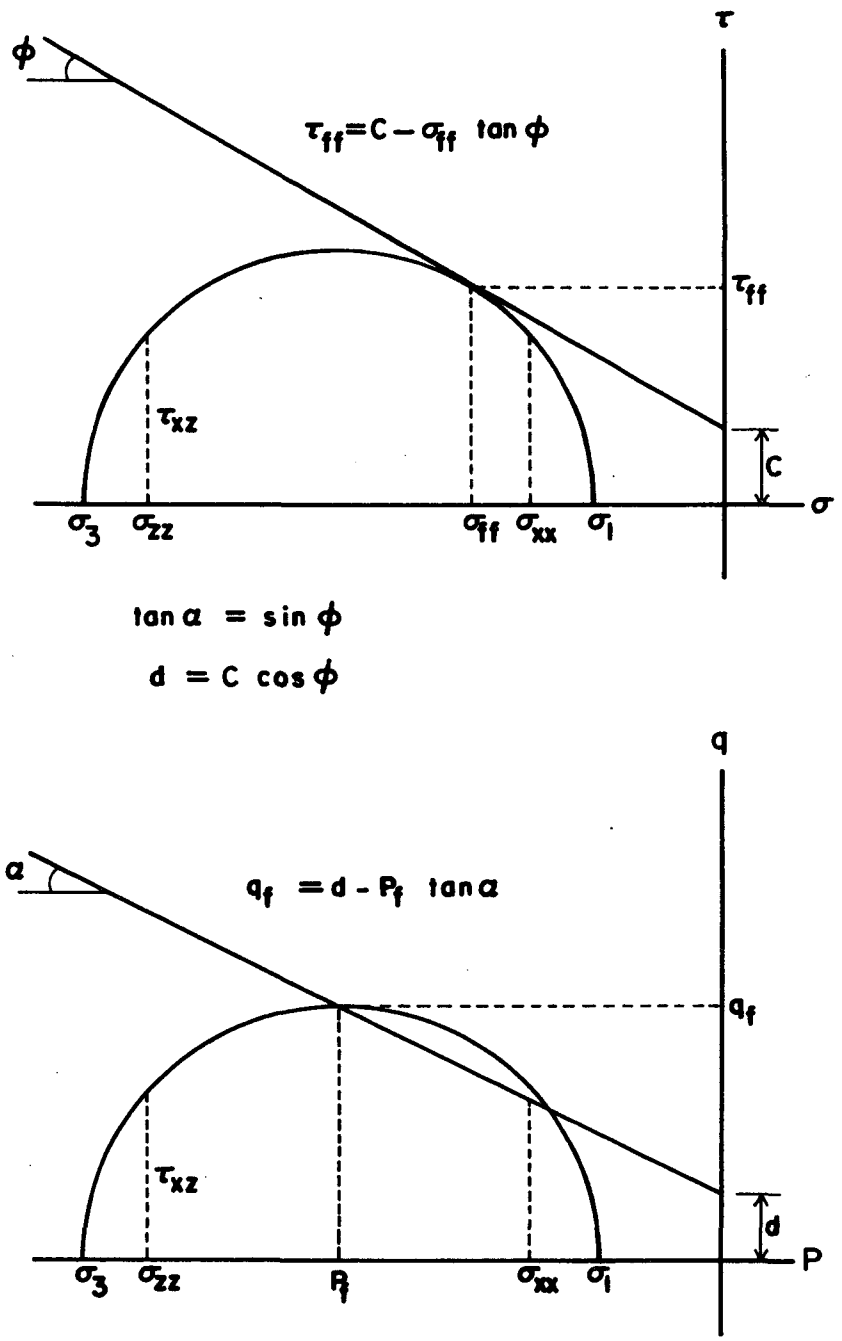

FIGURE 2.1 : MOHR–COULOMB FAILURE LAW AND MOHR'S CIRCLE

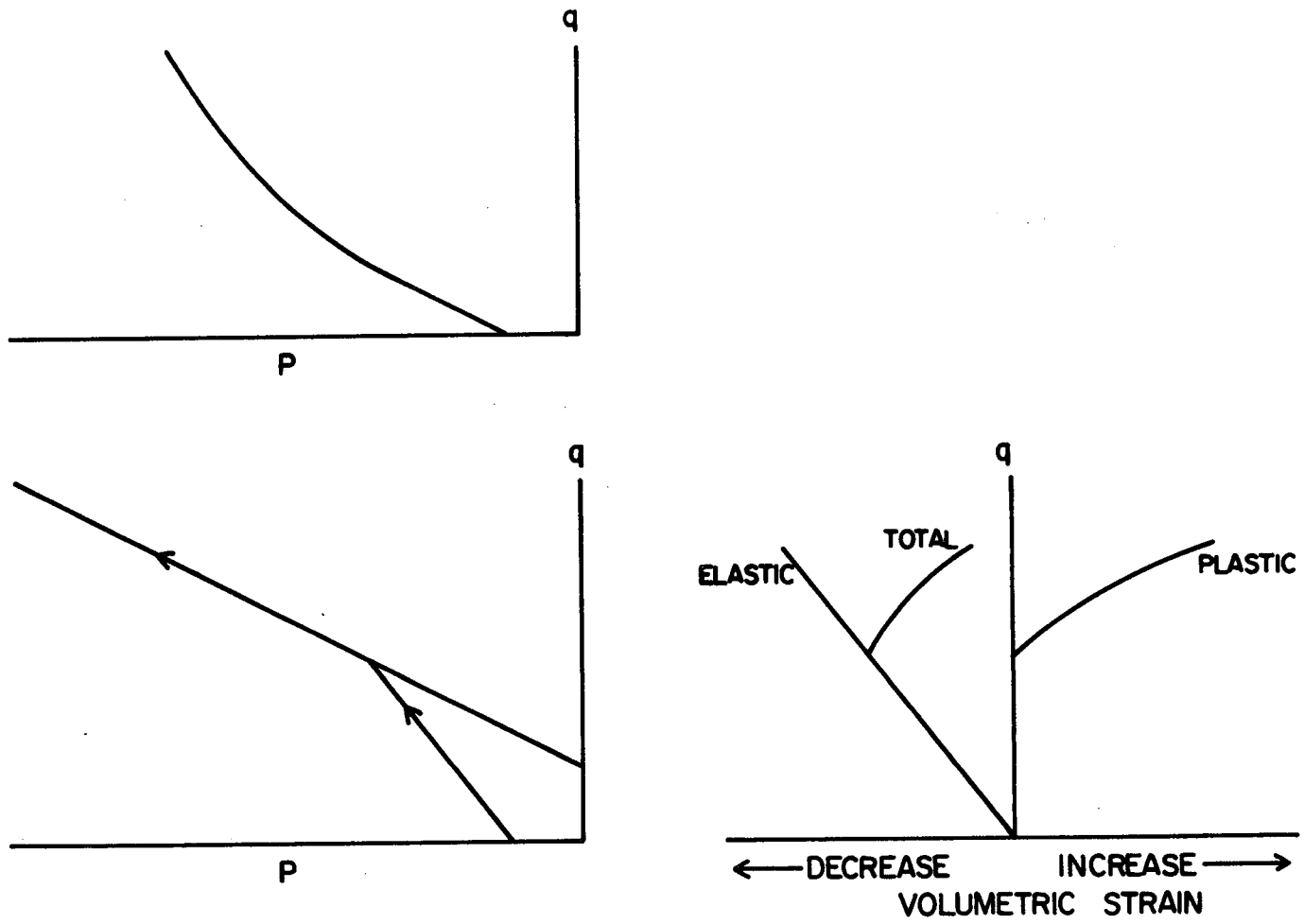

FIGURE 2.2 : STRAINS IN DILATANT MODEL

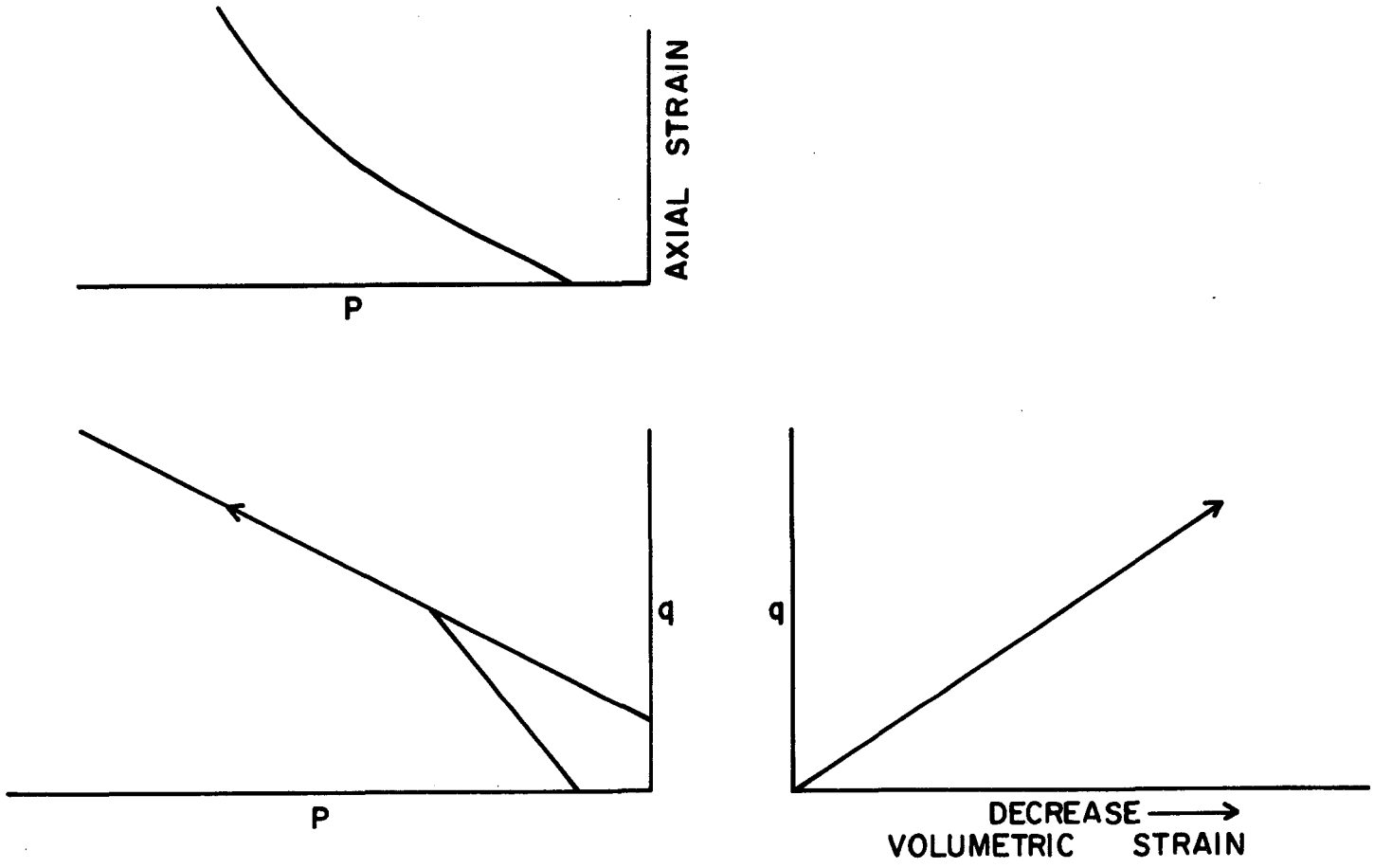

FIGURE 2.3 : STRAINS IN NONDILATANT MODEL

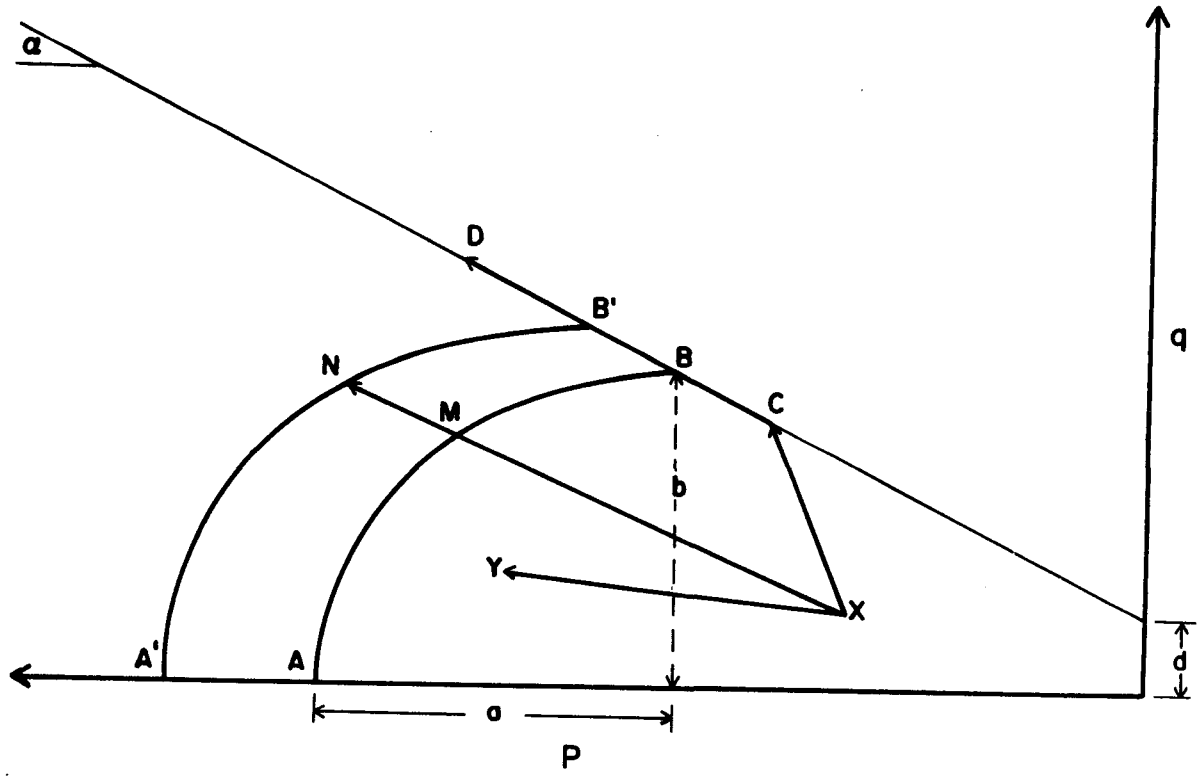

FIGURE 2.4 : STRAIN HARDENING YIELD SURFACE

CHAPTER 3

IMPROVEMENT OF FINITE ELEMENT SOLUTIONS

Finite element methods are numerical solutions of the differential equations governing the behavior of a material. The accuracy of the solution and the ease with which it is obtained are dependent on the numerical techniques employed to describe and solve these equations. This chapter will investigate several methods of improving the solution of a problem without greatly increasing the difficulty or cost required to obtain that solution. Modifications which have been made to the dilatant, non-dilatant, and strain hardening models to improve their solutions are described.

3.1 Correction of Stresses Which Exceed the Yield Criterion

The application of a load increment to nodes of the finite element model produces a corresponding stress increment for each element which is added to the stress existing in that element. As a result, the incremental stress may change the stress state from one below the failure envelope to one above the envelope. Implicit in the failure or yield criterion is the requirement that such a stress state cannot exist. Therefore, a correction has to be applied to reduce the computed stresses to values that are compatible with the envelope. At the same time the strains must be

adjusted to satisfy the stress-strain relation.

One technique to do this correction is to subdivide the load increment into fractions such that elements which yield for the first time during this load increment end up on the failure envelope. Such a procedure is very time-consuming and was not used in this work. The common technique and the one employed in this report is to correct only the stresses so that they lie on the yield surface at the end of the load increment. This procedure is not entirely satisfactory because it produces errors in the strains and non-equilibrium in the stresses of adjacent elements. However, these difficulties can be overcome by analyzing each load increment more than once. Reanalyzing each load increment, a process known as iteration, generally reduces the errors in the strains and the non-equilibrium in the stresses. In this report an iterative procedure which is discussed in detail in Section 3.2 is combined with the stress correction technique to produce stress states which satisfy the failure law and are close to equilibrium.

Three different methods were developed to correct stress states which exceed the failure envelope. Method 1, called MOCO 1, reduces the maximum shear stress, q, to a value compatible with the failure criterion while maintaining p constant. Method 2, MOCO 2, corrects the stress state back along a path perpendicular to the Mohr-Coulomb failure line.

Method 3, MOCO 3, corrects the stress state assuming the vertical stress remains constant. Figure 3.1 illustrates the correction paths for each of these techniques. The equations for the corrected stresses are derived in Appendix B.

A smooth retaining wall and a rigid footing were analyzed with each of these correction procedures to determine which method would produce the best solution. The finite element meshes, or grids, are shown in Figures 3.2 and 3.3.

The passive earth pressure for a dry cohesionless soil on a smooth wall of height H can be found from Rankine's earth pressure theory and is

$$P_p = \frac{\gamma}{2} \frac{1+\sin\phi}{1-\sin\phi} H \qquad (3.1)$$

where

P_p = passive force

ϕ = angle of internal friction of soil

γ = unit weight of soil

For a ϕ of 30°, γ of 2.0 TSM, and H of 10 M, P_p is 300T. Figure 3.4 shows the results of three solutions using the non-dilatant model with the three different correction procedures. Since both the Rankine theory and the non-dilatant model assume that failure is controlled by the Mohr-Coulomb failure envelope, they should yield the same passive

force at failure. Methods 1 and 2 overestimate the Rankine failure force by 6.7%; whereas Method 3 is in perfect agreement. The horizontal and vertical stresses at the end of each load increment are plotted in Figure 3.5 for elements 13, 14, and 15. For Methods 1 and 2, the vertical stresses at failure are higher than the initial vertical stresses. In an actual case the vertical stresses around the wall should not change with the horizontal loading of the wall. Method 3 produces vertical stresses at failure which are similar to the initial vertical stresses and in agreement with actual soil behavior.

No exact solution exists for the bearing capacity problem. Terzaghi developed a solution from limiting equilibrium that is conservative but provides useful results. Figure 3.6 presents the load-displacement curves for a rough, rigid footing loaded to failure using the three correction techniques and the non-dilatant model. The ultimate bearing capacity for this case using Terzaghi's bearing capacity factors is 150 TSM. Methods 1 and 3 yield similar results and predict failure at an average footing stress of 300 TSM. Chapter 4 will consider what the actual bearing capacity should be; however, it is readily apparent that Method 2 is producing an unreasonable solution after a displacement of 0.12 M. For elements outside the loaded area in which the horizontal stress is larger than the vertical stress, Method

2 produces vertical stresses in elements which are significantly different from the overburden stresses. Adjacent elements are not in equilibium; consequently, an instability is introduced into the solution.

Considering these results, in which Method 3 worked best for the smooth retaining wall and Methods 1 and 3 worked best for the footing, Method 3 appears to be the best overall correction technique, and will be used in the remainder of this thesis.

3.2 Iteration Procedure

Due to the facts that:

1. elements may be come plastic during a load increment but the stiffness coefficients remain elastic until the next increment;
2. stress states which exceed the yield criterion are reduced, inducing non-equilibrium in stresses between elements;
3. strains do not satisfy the stress-strain relation for the corrected stresses,

elements do not satisfy the requirements specified in Chapter 2 for the finite element method. As a result errors are induced in the computed stresses and strains. If each load increment is analyzed more than once these errors will usually be reduced.

An iteration procedure and convergence criterion have been added to the dilatant, non-dilatant, and strain hardening models to analyze each load increment more than once in order to improve their solutions. The convergence criterion requires that the corrected maximum shear stress, q, not differ from the uncorrected maximum shear stress by a specified percentage. This is one way of requiring that the element stresses be close to equilibrium. After each increment and for each element the convergence criterion is checked. If it is not satisfied, the element stiffnesses are recalculated, changing those which yielded during the previous iteration to plastic. The equilibrium equations are reassembled and solved for new strains. Stresses are recomputed and the convergence criterion checked. This process continues until the solution either converges or a specified number of iterations are completed, and then the next load increment is applied.

Figure 3.7 illustrates the effects of additional iterations on the solution of a rough, rigid footing. For a given displacement one iteration reduces the average stress acting on the footing, or in other words, for a given average stress on the footing one iteration increases the displacement of the footing. The additional iteration causes elements which have yielded to have plastic rather than elastic stiffness and produces larger displacements. Three

iterations give essentially the same result as two iterations for this case except after failure.

Reducing the size of the load increment will also reduce the errors in stresses and strains. Figure 3.8 compares the original solution to those obtained by doing one iteration for the same load increment size and obtained by halving the load increment size. Both of the latter require about the same computation time. Which solution is more correct will be discussed in Chapter 4. The main point is that a better solution can be obtained by reducing the load increment size or by increasing the number of iterations.

3.3 Effect of Number of Elements

Increasing the number of elements used to model a problem and the corresponding increase in the number of nodes usually leads to a better solution for the stresses and displacements. Adding more nodes increases the flexibility of the entire system. Adding more elements produces a better definition of the stress distributions especially at stress concentrations. Many authors including Clough et al. (1965) have shown this behavior to be true. However additional nodes and elements increase the amount of computer time and the computer storage space required to solve the equations, usually by an amount exceeding the increase in the number of nodes and elements. There is

an economic advantage in reducing the number of nodes and elements as much as possible and still maintain an acceptable solution.

Figure 3.9 illustrates the results of increasing the number of elements from 30 to 96 to model a rigid footing while maintaining all other variables, including the lateral boundaries, constant. These results are from the non-dilatant model with a frictional material. The surprising result is that with three times as many elements, there is not much difference in the solution. Similar results have been obtained for a retaining wall using 64 and 145 elements. The exact solution of this problem is unknown; however, one can conclude that for the purpose of doing comparisons of the various constitutive relations and solution procedures in a homogeneous material, a relatively small number of elements is sufficient.

3.4 Tensile Elements

In the non-dilatant and dilatant models surface elements to the side of a footing, or in front of a retaining wall loaded passively, tend to become tensile, i.e., the stresses become positive. Drained soil cannot sustain tensile stresses, and cracks form. However, the present finite element formulation will not allow such cracks to develop. Hagmann (1971) suggested that the stiffness of tensile

elements be reduced and their stresses set equal to zero. In general variations of this method caused his solutions to become methematically unstable.

This procedure was carefully reconsidered. In Hagmann's method, each time an element became tensile, its stiffness was reduced. If in a subsequent increment the same element became tensile, the stiffness was again reduced. This procedure soon reduces an element's stiffness to the point where the global stiffness matrix becomes ill-conditioned and solution by Gaussian elimination produces large errors.

The method adopted in this work is to reduce a tensile element's stiffness only once, require the element stiffness to maintain that value for all subsequent load increments, and set the stresses equal to zero. If in subsequent increments, the element again becomes tensile only the stresses are set equal to zero. In Figure 3.10 the results of run HS, Figure G-6 of Hagmann (1971) are reproduced along with the results of an identical run with the above modification to treat tensile elements. The mathematical instability found by Hagmann does not occur using this procedure.

3.5 Interpretation of Nodal Forces

In the finite element method forces are computed at each node which correspond to the external loads applied to the model and the internal stresses in the elements. The

load on a wall or footing will be the sum of the forces acting at the individual nodes comprising that wall or footing, e.g. nodes 18, 19, 20, 21, 22 in Figure 3.2 and nodes 6, 12, 18, in Figure 3.3. Incremental nodal forces are computed from the incremental strains and element stiffnesses. They are then summed to find the total load acting on the structure. However, as was discussed in Section 3.2, the incremental strains and element stiffnesses may contain errors. Consequently, the incremental nodal forces will be in error, and the computed load acting on the structure will become more incorrect with each additional load increment.

In addition high stress concentrations exist around node 18 in Figure 3.2 and node 18 in Figure 3.3. These increase the forces acting on that node. In an actual case a wall would slide away from node 18 or cracks would develop at the edge of the footing, but these deformation modes cannot occur in the finite element model. As a result, the computed nodal force at stress concentrations like node 18 are too large.

The force acting on a structure may also be computed from the stresses in the elements adjacent to the structure. Since the stresses are required to conform to the yield criterion, it might be expected that a better estimate of the failure load could be obtained from the stresses than from the nodal forces. Indeed this is the case as shown in

E

Figure 3.11 for a retaining wall. The curves obtained from the stresses are the same as those shown in Figure 3.4 and yield a good estimate of the failure load. However, the curves obtained from the nodal forces greatly overestimate the failure load due to the errors in the nodal forces discussed above.

The error in the nodal forces can be reduced by decreasing the error in the strains, e.g. by increasing the number of iterations per load increment or reducing the load increment size. A larger number of elements will better define the stress values at stress concentrations and produce more correct values of nodal forces at those points. Figure 3.12 demonstrates that these refinements do reduce the difference between the total load computed from nodal forces and that computed from adjacent element stresses. However, since good estimates of failure loads can be obtained from the element stresses, the additional computation time and expense necessary to obtain more correct nodal force values seems unwarranted. For the remainder of this thesis, only loads obtained from the stresses in elements adjacent to a structure will be considered.

3.6 Reduction of Core Storage Requirements

Finite element solutions to practical problems can be expensive. Minor revisions to a program's mode of operation

may sometimes result in significant cost reductions. In finite element programs, computer cost has two major components, core storage requirements and computing time. Several matrices in the programs have values which are used more than once in the analysis. A decision must be made whether to store these values as they are computed for later use, which requires greater computer storage space, or recompute values as they are needed, which requires additional computation time. This decision is based on the relative cost of storage space and computation time.

For the computer system currently in use at M.I.T., IBM 370-M155-MVT, it is cheaper to recompute values for the large matrices in these programs as they are needed. For other computing systems, the opposite may be true, and the programs should be adjusted accordingly.

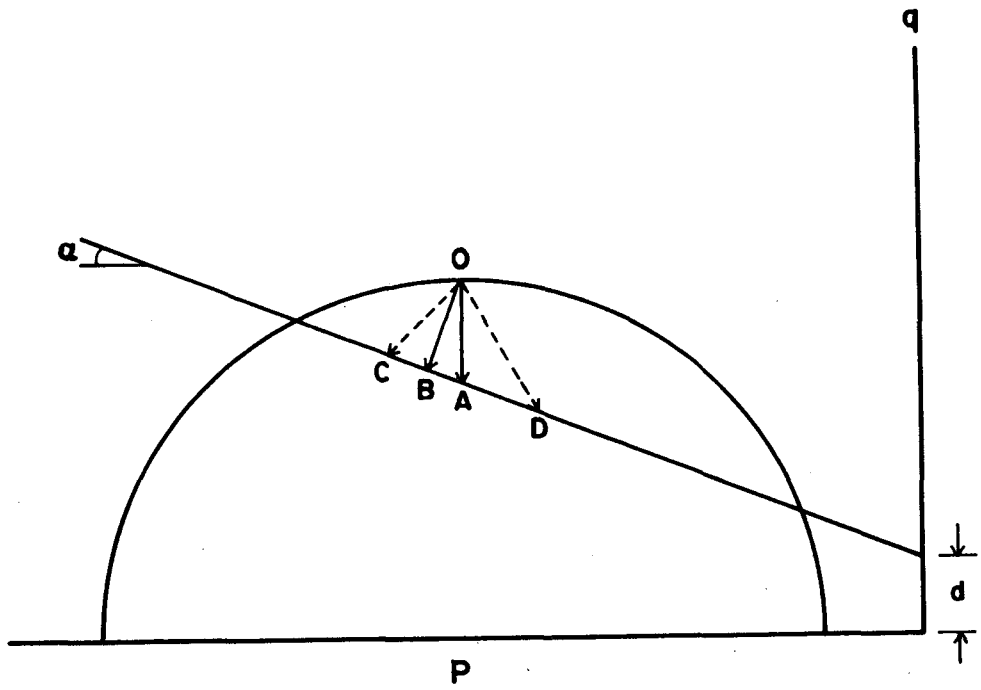

$\overline{OA}$	direction	of	correction for	MOCO 1
$\overline{OB}$	direction	of	correction for	MOCO 2
$\overline{OC}$	direction	of	correction for	MOCO 3 , $\sigma_v > \sigma_h$
$\overline{OD}$	direction	of	correction for	MOCO 3 , $\sigma_h > \sigma_v$

FIGURE 3.1 : CORRECTION PROCEDURES FOR STRESS STATES EXCEEDING MOHR-COULOMB LINE

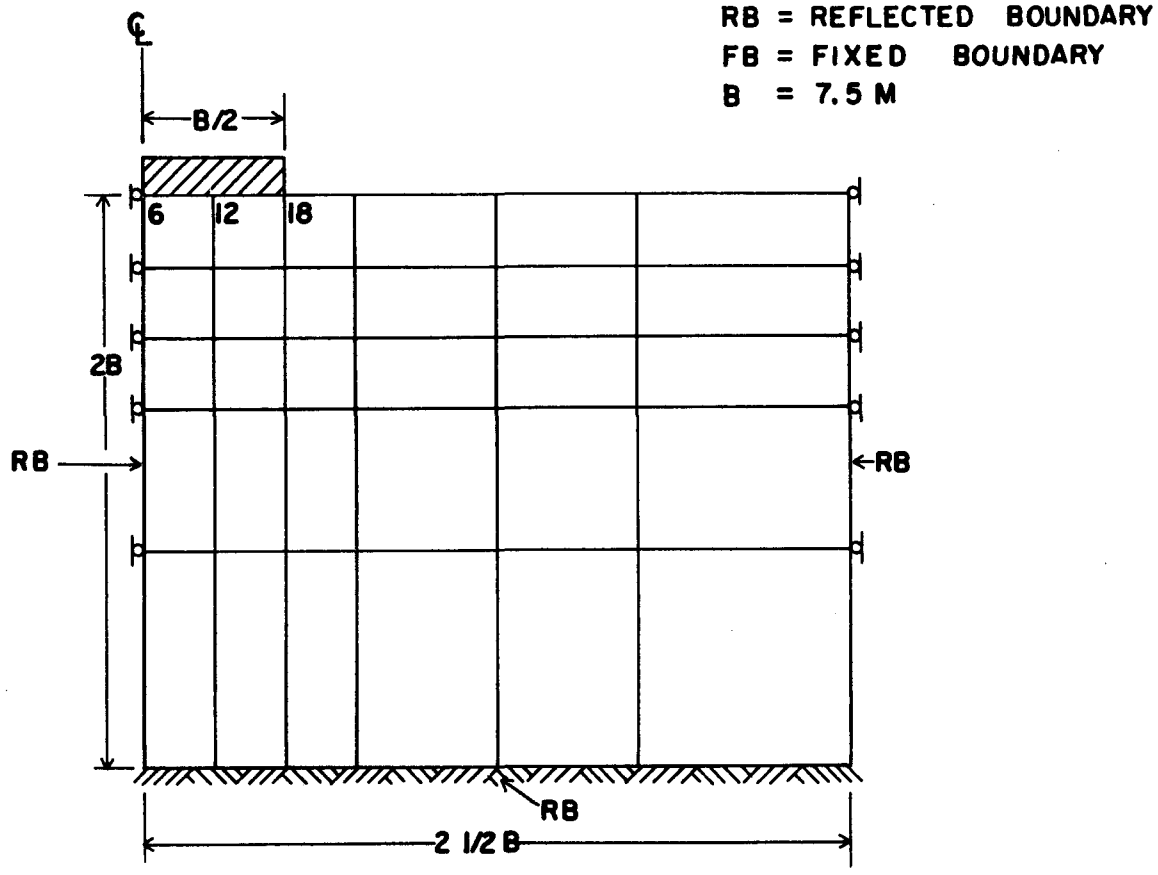

FIGURE 3.2 : STANDARD FOOTING GRID

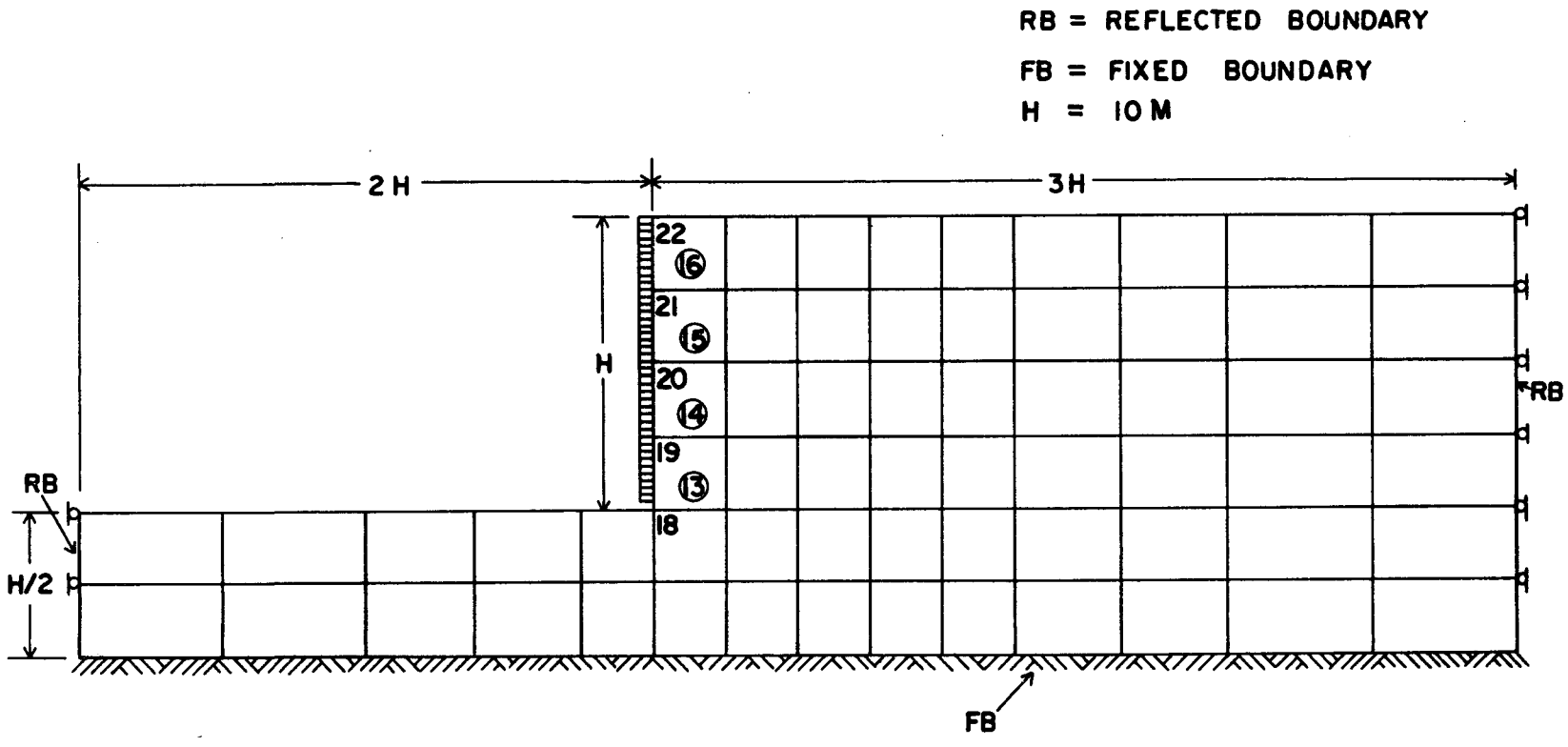

FIGURE 3.3: STANDARD RETAINING WALL GRID

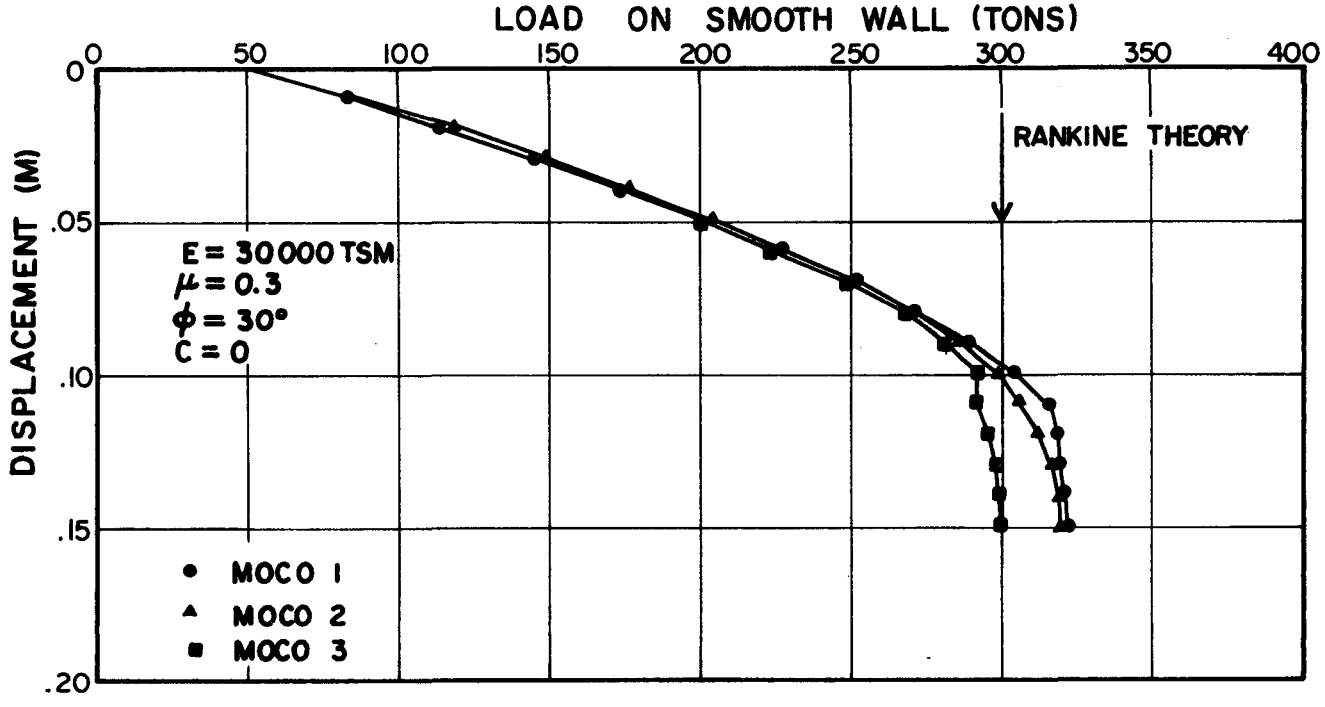

FIGURE 3.4 : SOLUTIONS FOR RETAINING WALL USING THREE CORRECTION PROCEDURES

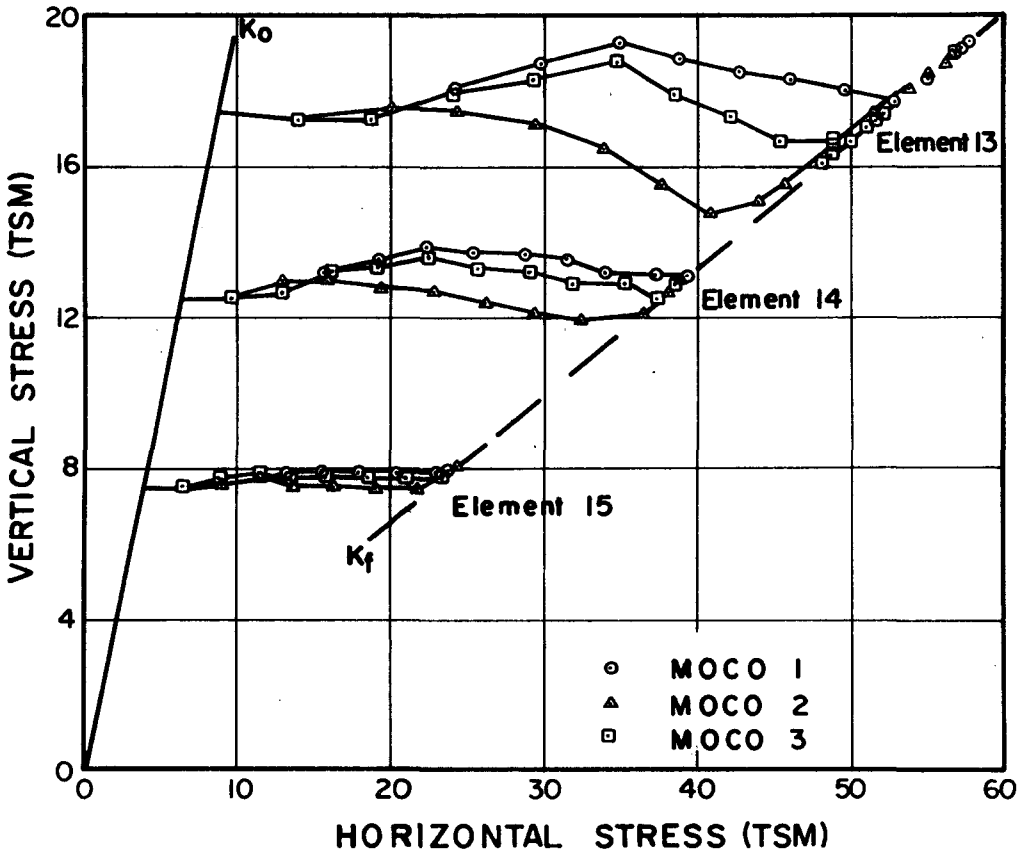

FIGURE 3.5 : STRESSES BEHIND RETAINING WALL

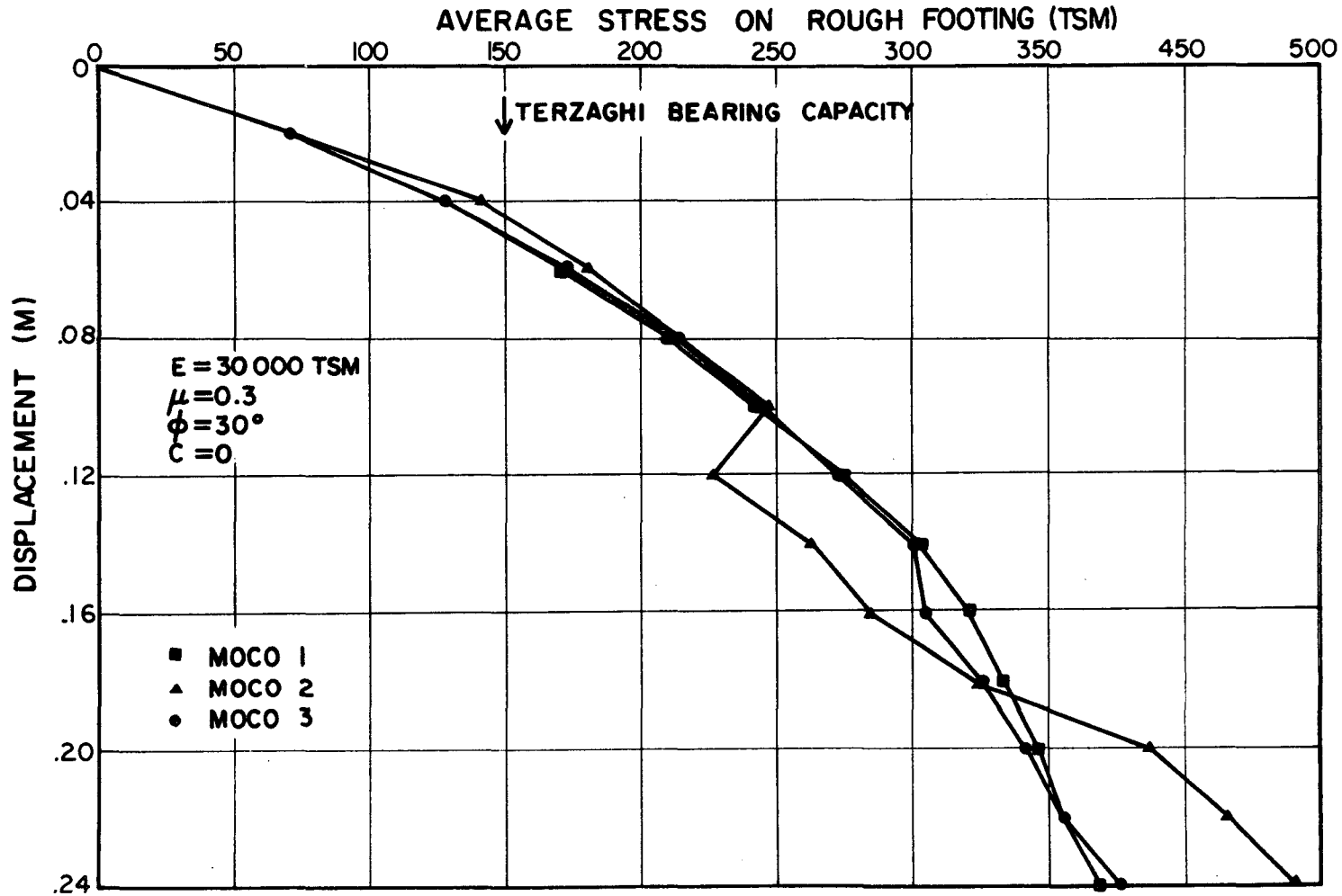

FIGURE 3.6 : SOLUTIONS FOR RIGID FOOTING USING THREE CORRECTION PROCEDURES

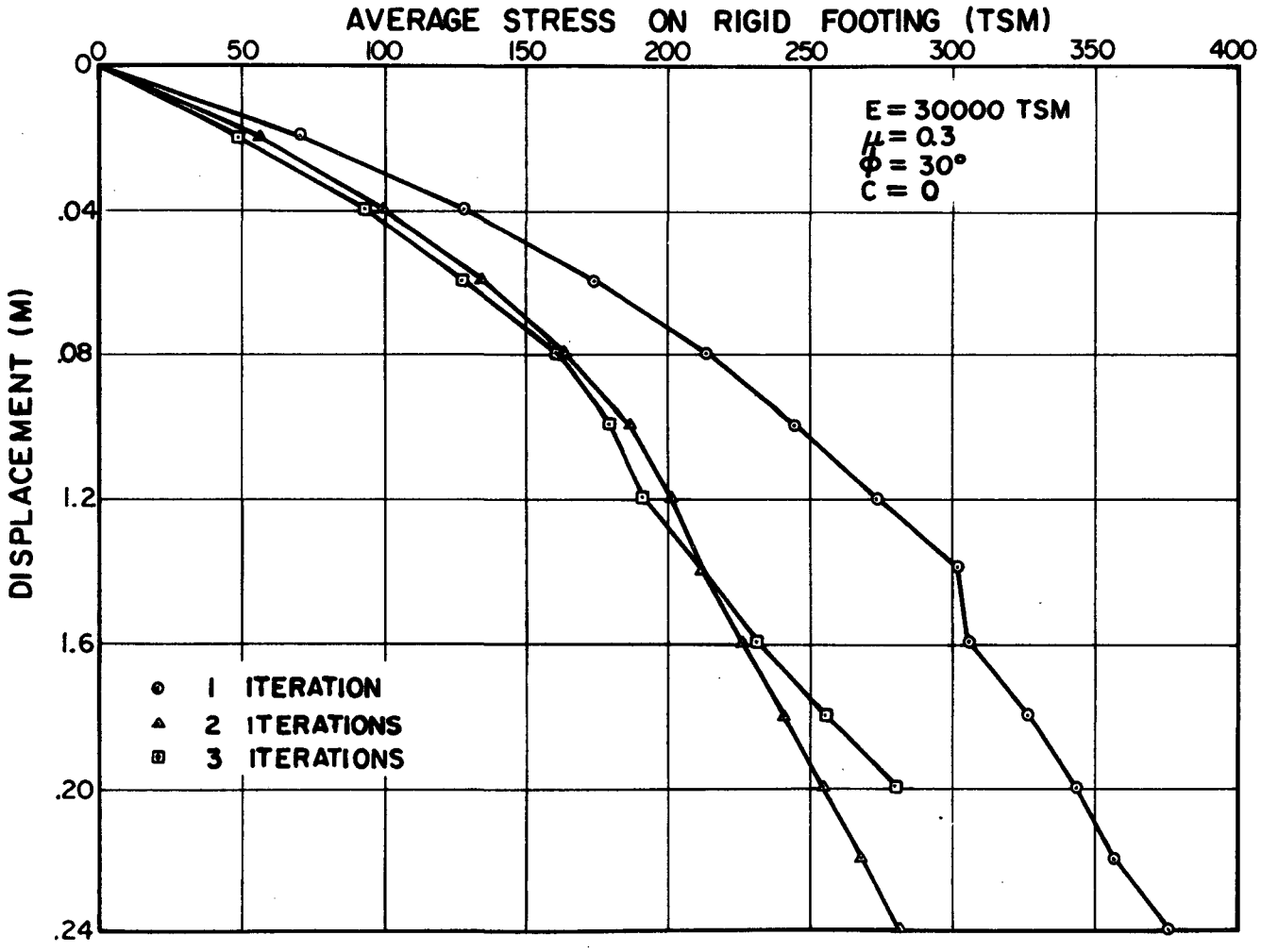

FIGURE 3.7: EFFECT OF NUMBER OF ITERATIONS ON LOAD DISPLACEMENT CURVE

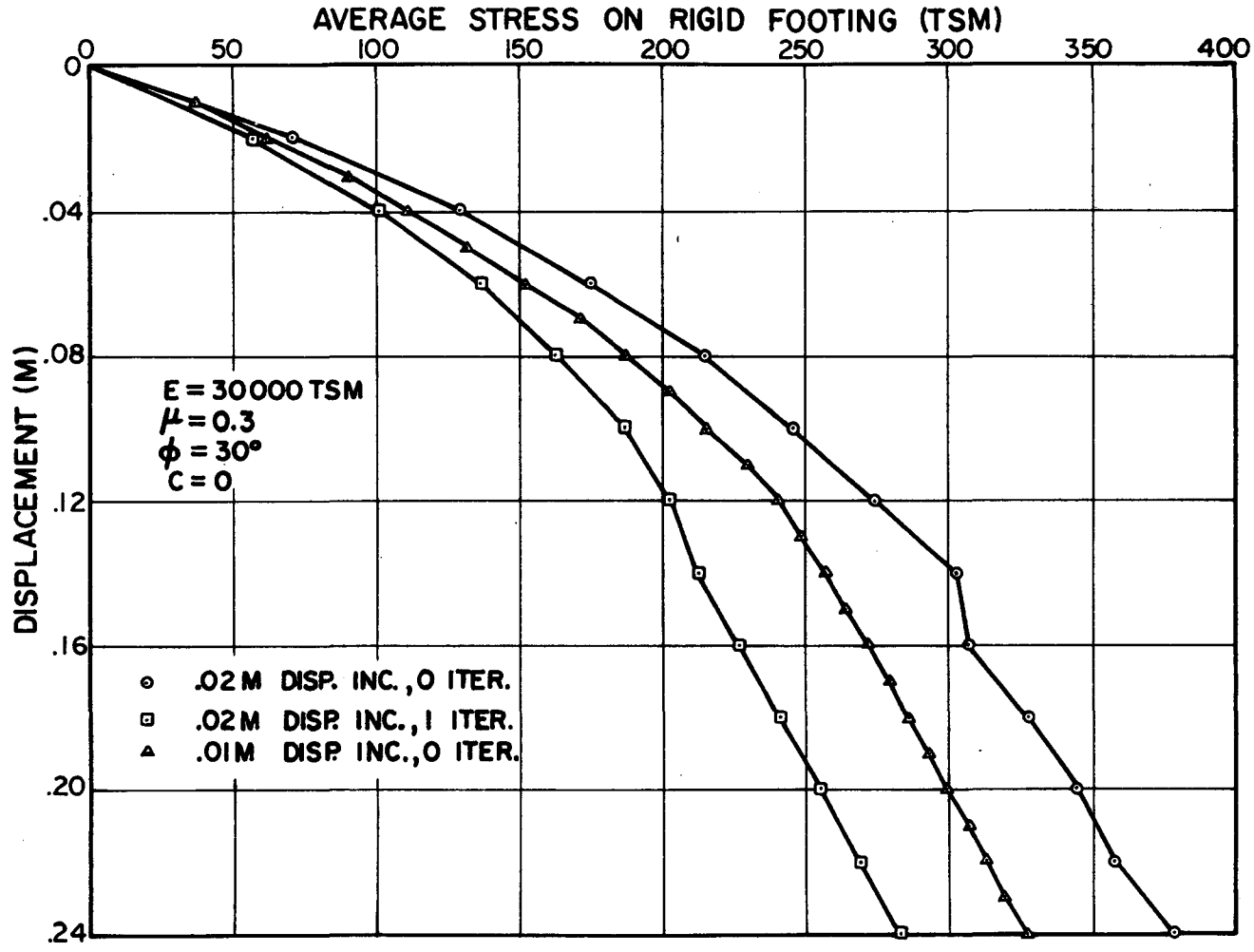

FIGURE 3.8 : EFFECT OF REDUCED LOAD INCREMENT SIZE ON LOAD DISPLACEMENT CURVE

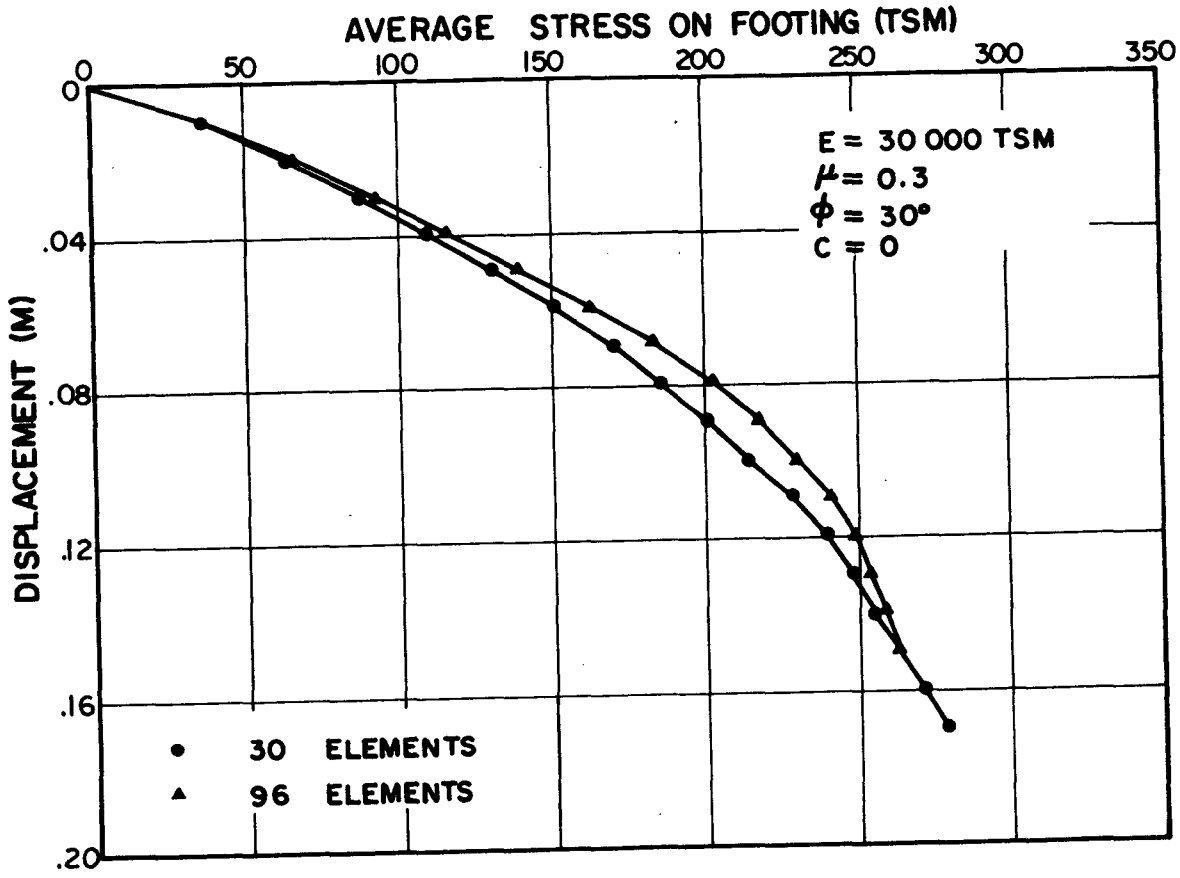

FIGURE 3.9: EFFECT OF NUMBER OF ELEMENTS ON LOAD DISPLACEMENT CURVE

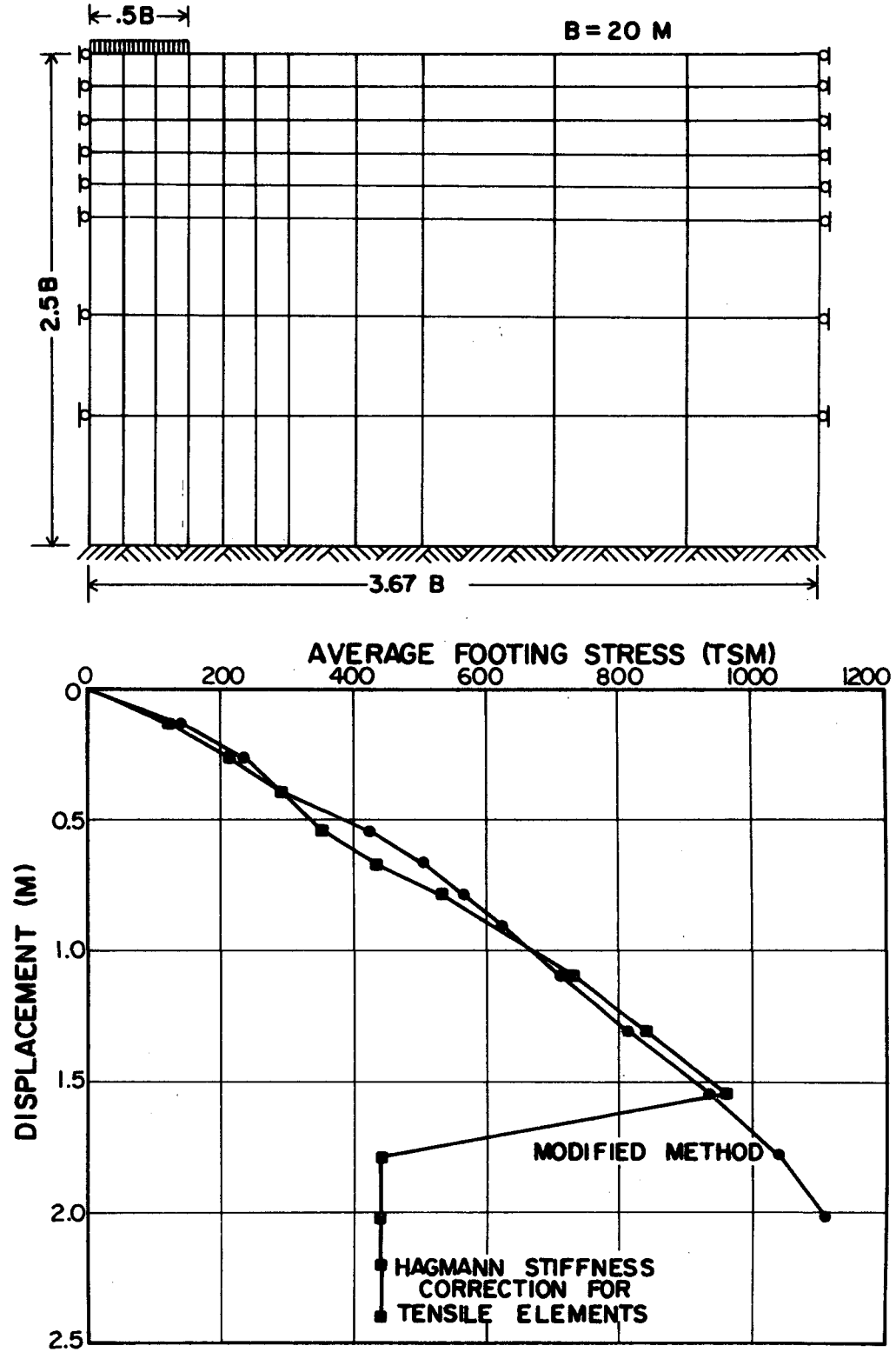

FIGURE 3.10: BEHAVIOR OF ELEMENTS IN TENSION

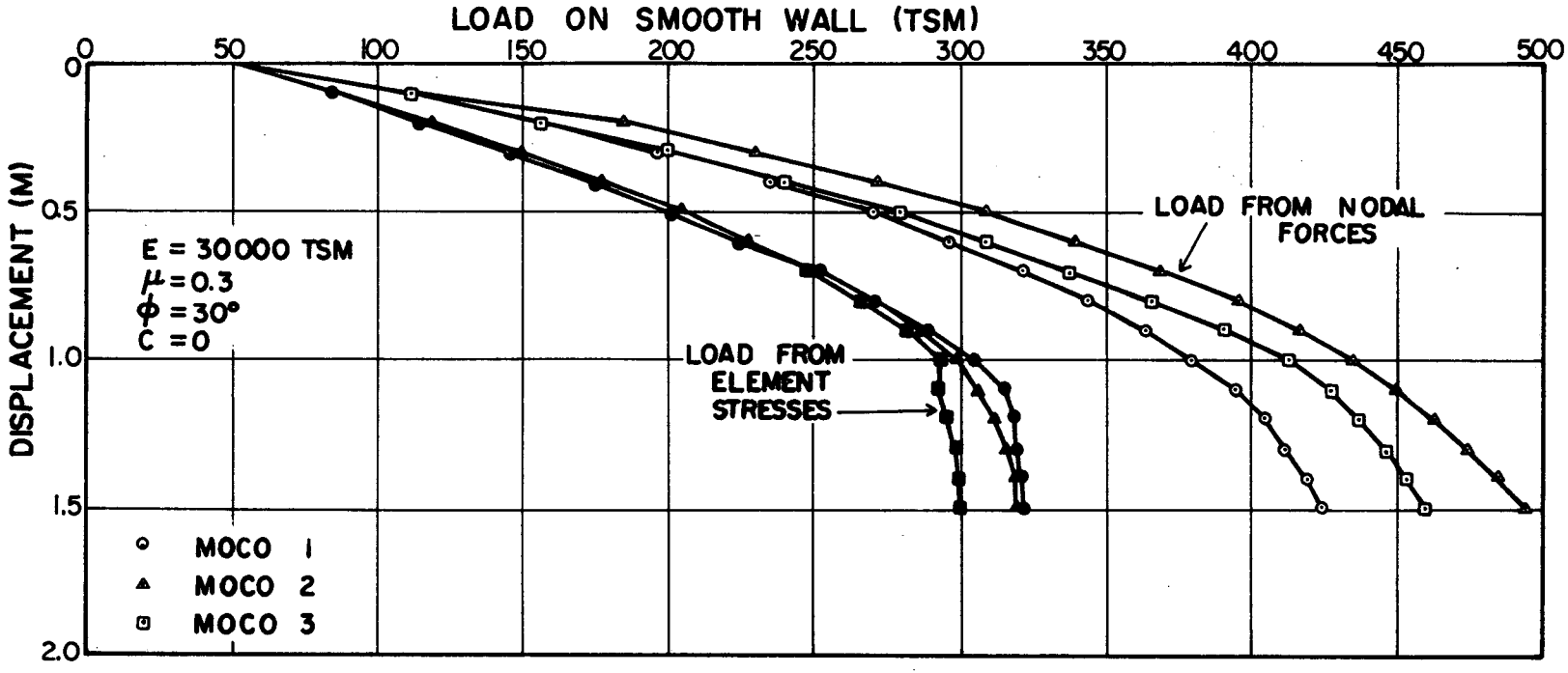

FIGURE 3.11 : ERROR IN NODAL FORCES

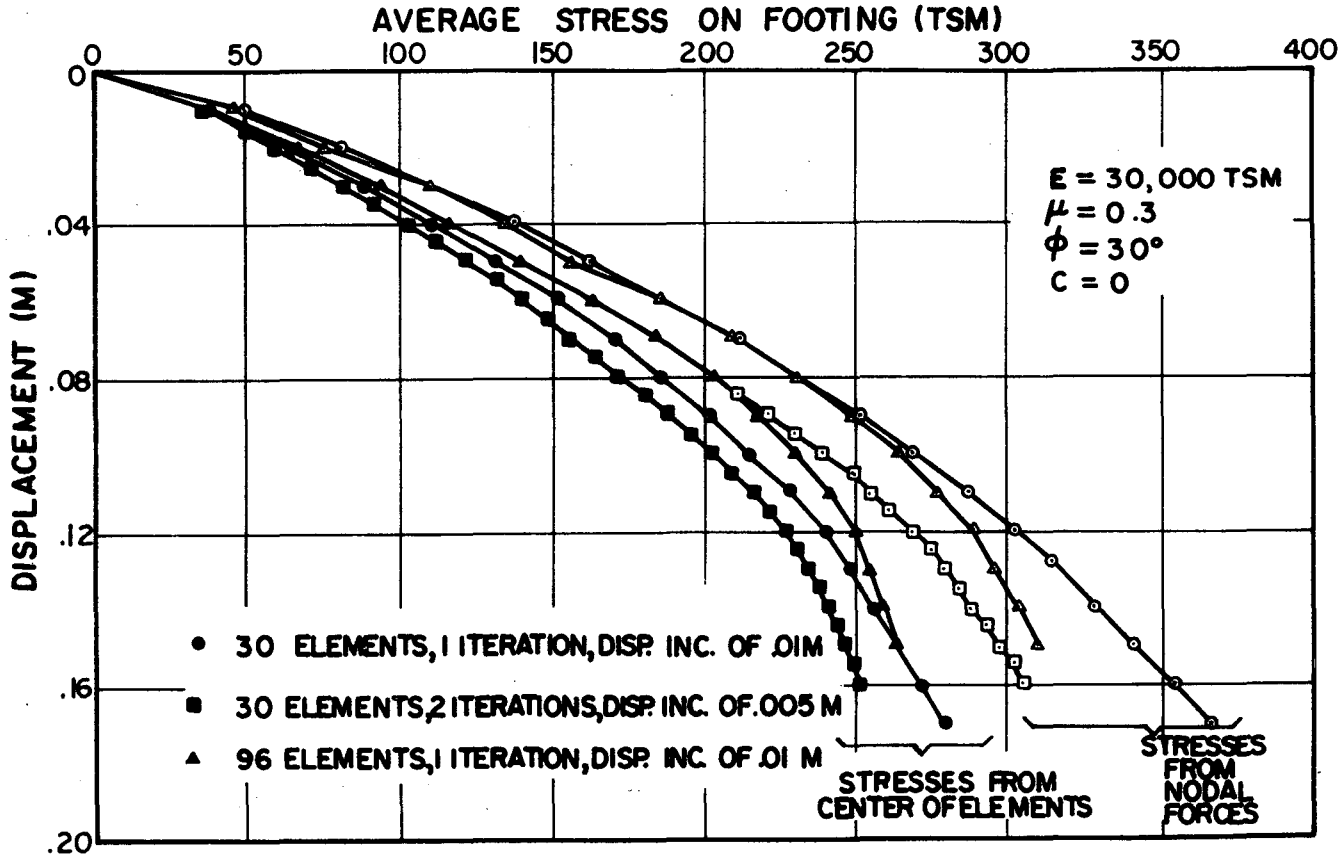

FIGURE 3.12: DECREASE OF ERROR IN NODAL FORCES

CHAPTER 4

SOLUTIONS FOR RETAINING WALLS AND FOOTINGS

Two problems frequently encountered in soil mechanics are those of determining the ultimate loads that can be imposed on retaining walls and footings. From the theories of plasticity, limit analyses and extremum methods, analytical solutions have been obtained which predict the loads that cause failure of retaining walls and footings. In this chapter finite element programs employing the five constitutive relations discussed in Chapter 2 are used to solve retaining wall and footing problems. The results of the finite element solutions are compared with their analytic counterparts to investigate the predictive ability of the constitutive relations.

4.1 Retaining Walls

Failure of retaining walls is one of the easier analytical problems in soil mechanics. Coulomb (1776) developed a formula for the earth pressure acting on a retaining wall by assuming straight lines of rupture. Later Rankine (1857) developed his well known formula for active and passive states of failure. These two theories remain in wide use today despite their limitations and the later developments of Kötter (1903), Janbu (1957), Sokolovski (1965),

Hansen (1953), and others. These methods have been adequately described elsewhere and only their results will be included in this thesis. See Hansen (1953) and Sokolovski (1965) for an excellent review of these and other retaining wall solutions.

All analyses in this section are done using the standard retaining wall grid shown in Figure 3.3 unless otherwise noted. This grid was developed to model the problem sufficiently with a minimum of elements in an effort to reduce computation costs.

4.1.1 Non-dilatant Material

The load displacement curves obtained for rigid horizontal translation of a smooth retaining wall in dry cohesionless soil using the non-dilatant material are shown in Figure 4.1. Load is expressed as an earth pressure coefficient, K, which is defined as the horizontal load on the wall divided by $.5\gamma H^2$. Table 4.1 summarizes the soil parameters used for these and subsequent finite element solutions for retaining walls. The active and passive failure loads predicted by the non-dilatant model are exactly those obtained from Rankine's earth pressure theory. This result is to be expected since both analyses make the same basic assumption, i.e., the soil behind the wall fails and can gain no additional shear stress once the stress state

reaches the Mohr-Coulomb failure envelope.

Figures 4.2a and 4.2b show typical yield patterns at failure for the active and passive cases respectively. The top row of elements behind the wall all fail at very low displacements. These elements have low horizontal and vertical stresses at the onset of loading, and a small displacement of the wall load causes them to yield. An active state develops in front of the wall for passive loading. Cracking and sliding would hinder the development of such a large active zone in a field case. The close proximity of the rigid bottom boundary produces a yielded zone beneath the wall. From these results one can see that although this relatively coarse mesh produces a somewhat unreasonable picture of the yield zones at failure, a good estimate of the failure load is obtained. A more realistic yielded zone can be obtained by using a larger mesh with more elements.

Horizontal loading or unloading produces no abrupt rotation of principal planes ; consequently a good finite element solution can be obtained with one iteration. As will be shown in Section 4.2, loading of footings does produce abrupt principal plane rotations and more iterations per load increment or smaller load increments become necessary.

Friction between the wall and soil increases the load required to cause passive failure and reduces the load required

to cause active failure. Figure 4.3 illustrates this fact for the case where the friction angle between the soil and wall equals that of the soil. For the non-dilatant model wall friction increases the passive failure load to 188% of the Rankine passive force and reduces the active failure load to 82.5% of the Rankine active force. These values are constitent with those presented in Table 4.2 which summarizes the results of several failure theories for the case where the wall friction angle equals that of the soil. The displacements required to cause failure are 4 to 5 times larger for a rough wall than for a smooth wall.

Active and passive failure states may also be reached by rotating the wall about its bottom or top. The solid lines in Figure 4.4 show the change in earth pressure coefficient as a wall is rotated about its base. The dashed lines are the results for horizontal translation, Figures 4.1 and 4.2, replotted. For rotation, Y is defined as the displacement at midheight of the wall, so that a given Y implies the same volume of soil displaced in rotation as in translation. From these results it is apparent that for rotation about the wall base much larger displacements are necessary to develop fully failure than for horizontal translation. The larger displacements are necessary to develop sufficient strains in the elements at the wall base to cause them to yield.

In an actual case, pure rotation about the wall base can never be practically achieved. There will always be some translation which may change considerably the amount of rotation necessary to fully develop the active or passive resistance along the wall.

4.1.2 Dilatant Material

Figure 4.5 illustrates the values of earth pressure coefficient for horizontal translation of a rough and smooth retaining wall in dry cohesionless soil using the dilatant model. The smooth, passive earth pressure coefficient at failure is 3.2 or 6.7% greater than the Rankine passive failure coefficient. The smooth active coefficient is .32 of 97% of the Rankine value for a smooth wall. The rough, passive earth pressure coefficient is 6.42 or 214% of the Rankine smooth wall passive value and is similar to the higher values given in Table 4.2.

The smooth active earth pressure coefficient obtained from the dilatant material is 97% of that obtained from the non-dilatant material. The smooth, passive value for the dilatant material is 107% of that for the non-dilatant material while the rough, passive value is 110% greater. These differences are consistent with the fact that the dilatant model expands in volume when sheared which results in higher shearing resistance and

increase the load required to cause failure. The largest strength increase due to dilatancy occurs in the rough, passive case where it is to be expected that the shearing stresses developed in the soil will be greatest.

4.1.3 Strain Hardening Material

The results for the strain hardening model for a smooth wall in horizontal, passive translation are shown in Figure 4.6. There is an abrupt change in the slope of the load displacement curve at a K of 1.56 which is due to most of the elements in the mesh developing stress states which exceed their respective capped yield surface. In the strain hardening model, elements which reach a stress state on the Mohr-Coulomb failure line deform the same way as elements which reach a stress state on the capped yield surface. There is no provision for an element to fail plastically. Consequently, the elements behind the wall continue to deform without ever failing as shown in Figure 4.6.

4.1.4 Hyperbolic and Tresca Materials

Molina (1971) has investigated the retaining wall problem using the hyperbolic and Tresca large strain models. His results are in agreement with those presented here (with the exception of the strain hardening model).

Excellent solutions for the horizontal earth pressure on a retaining wall can be obtained from these finite element models. Of course, one can obtain good solutions for the failure loads without the finite element method. The sole reason that they are considered here is to provide concrete evidence that the finite elements programs do analyze the stress-strain behavior of soil correctly.

4.2 Strip Footing on Frictional Material

Prediction of the load required to cause a bearing capacity failure of a strip footing is much more complicated than prediction of the failure load for a retaining wall. Combining the effects of gravity, friction and cohesion make exact analytical solutions impossible without making simplifying assumptions. Bearing capacity factors obtained by Terzaghi are commonly used for predicting the ultimate load a footing may carry even though they are known to be considerably conservative (Lundgren and Mortensen (1953) and Gorbunov-Possadov (1965)). Other solutions have been obtained (see Reddy (1970)) but which one is more correct is uncertain. In this section the failure of a footing on dry cohesionless soil will be investigated. Only rough, flexible and rough, rigid footings are considered. As will be shown, the solution of a footing problem is much more dependent on the load increment size and the

number of iterations per load increment than was the retaining wall problem.

The standard footing grid shown in Figure 3.2 is used for the computer solutions unless otherwise noted. Since the problem is symmetric about the centerline of the footing only half of the geometry is required. This grid is too coarse to give the most correct finite element solution; however, there are a sufficient number of elements to provide solutions which can be used for qualitative evaluation of the solution procedures and the constitutive relations. Table 4.3 summarizes the parameters used for the footing problems.

4.2.1 Non-dilatant Material

Figure 4.7 contains four displacement curves for loading of a rough, rigid footing on dry, cohesionless soil. The number of iterations per load increment and the size of the load increments were varied to determine their effect on the load-displacement solution. Run 21 was loaded with displacement increments of .02 M and no iterations. Run 22 is similar to Run 21 except one additional iteration was performed per load increment. The additional iteration produces a larger displacement at a given load, which is the result of plastic strains in elements that yielded in that increment. With no iteration, plastic

strains do not occur in an element until the increment following that in which the element exceeded the failure criterion. An iteration produces plastic strains in the same load increment that failure was reached.

A large load increment size results in premature yielding of elements. The stress in an element may exceed the failure criterion during the large increment; whereas, several smaller increments which give the same load as the one large increment may produce a stress state below the failure line.

For the finite element solutions, bearing capacity failure is defined as the point where the load-displacement curve undergoes a significant change in slope. This definition is somewhat arbitrary; however, for frictional materials the finite element solutions never produce infinite displacements at some maximum load. Run 21 predicts failure at an average footing stress of about 300 TSM; whereas, Run 22 fails at 200 TSM.

The load increment size for Run 23 was half that of Run 21 and no iterations were performed. Failure occurs at 240 TSM. Run 24 has a load increment size one fourth that of Run 21 and one iteration. The displacement curve is much smoother and failure at 230 TSM is much better defined than in the previous results. It appears that

a displacement increment size less than $2.10^{-8} \cdot H \cdot E$, where H is the height of the finite element grid in meters, E is the modulus of elasticity of the soil in tons per square meter, and the increment size is in meters, is necessary to obtain a reasonable load-settlement curve for a footing with the non-dilatant model.

The failure load predicted by Terzaghi bearing capacity factors for this case is 148 TSM. The best estimate of the failure load from these solutions is 230 TSM; however, a better solution may be obtained with a larger mesh, smaller load increments, and more elements.

Figure 4.8 illustrates the yielded zones at various footing loads for Run 24. Contrary to the behavior of a purely cohesive or undrained material which fails when the yielded zone intersects a free boundary (Christian (1966)), a frictional material continues to develop additional shearing resistance once failure is reached. Consequently, the load-displacement curves never become vertical as is the case with a cohesive or undrained material. The yielded patterns shown in Figure 4.8 are very dependent on the grid used. Yielding at the bottom and right boundaries suggests that a larger grid is necessary to define better the development of the yield zones. A significant yielded zone develops at only 10% of the failure load. Since the soil starts out in a K_o condition very

little displacement is required to initiate yielding.

In Figure 4.9 a flexible footing, Run 25, is compared with a rigid footing, Run 24. Displacements of the rigid footing are intermediate between the centerline and edge displacements of the flexible footing. The flexible footing fails at a load of 212 TSM.

4.2.2 Dilatant Material

Once a dilatant material fails, large volumetric increases occur which lead to additional shearing resistance. Figure 4.10 shows the load-displacement curve for a rigid footing on a dilatant material. Run 26 does not exhibit a change in slope of the load-displacement curve that would indicate failure, even at stresses in excess of three times the Terzaghi bearing capacity value. Run 27 with a load increment size one fourth that of Run 26 gives essentially the same result. For the retaining wall problem the results for the dilatant model were similar (within 7%) to the non-dilatant model. The reason that the dilatant model is much stronger in the footing problem is that the boundary conditions are much more confining. With each load application, the average confining stress increases, the soil dilates, and additional shearing resistance is developed.

To investigate the confining effect of the boundary

conditions, the right vertical boundary of the grid was allowed to move freely, horizontally and vertically, in Run 28. Relaxation of the right boundary constraint produces a much softer, weaker material; however, the grid no longer models the typical bearing capacity problem for a confined soil. A larger grid with more elements will minimize the effects of the boundary constraints, but the strength of the dilatant model will remain much higher than that predicted by Terzaghi or the non-dilatant model as was shown by Hagmann (1971).

4.2.3 Strain Hardening Model

Figure 4.11a shows the solution of a rigid footing on the standard mesh using the strain hardening model. This model is much softer than either the dilatant or non-dilatant model and there is no point on the load displacement curve which can be defined as failure. Figure 4.11b shows the horizontal and vertical stresses for three elements as loading progresses. The stress behavior is very erratic which is due mainly to the way the strain hardening model treats elements on the failure line. Stress changes on the Mohr-Coulomb failure line produce the same type of strains as do stress changes on the elliptical yield surface in the present formulation.

An element is never allowed to fail plastically. Clearly, strains on the failure line should follow a different constitutive relation such as that in the dilatant or non-dilatant model.

4.2.4 Hyperbolic Material

The load displacement curve for a footing on a drained frictional material using the large strain hyperbolic model is shown in Figure 4.12. Results from the non-dilatant model are also shown for comparison. As the footing load is increased, the hyperbolic model becomes more stiff, and failure is never reached.

The present hyperbolic formulation computes an incremental shear modulus, G, which is a function of the ratio of the stress difference, $(\sigma_1-\sigma_3)$, and the confining stress, σ_3. The incremental bulk modulus, B, depends only on the confining stress, σ_3. As the material is loaded, G decreases and B increases. When B becomes considerably larger than G, Poisson's Ratio, μ, approaches 0.5 and the material becomes incompressible. Results obtained for a case in which B was kept constant and large compared to G were similar to Run 33. However, a small strain formulation where B was larger compared to G yielded results qualitatively similar to those for the non-dilatant material.

The large strain model appears to be very sensitive to large values of μ. More work is required to determine the effects of μ on the large strain hyperbolic formulation for a frictional material. A formulation which uses the elastic parameters E and μ instead of B and G or one which limits the largest value of B may be more desirable.

4.3 Strip Footing on Cohesive Material

For purely cohesive material the non-dilatant and dilatant plastic relations reduce to the Tresca perfectly plastic relations. Christian (1966) investigated the undrained behavior of the Tresca relations and found that the load at failure agreed well with values obtained from limiting equilibrium. The results of a flexible footing using the non-dilatant model are shown as Run 30 in Figure 4.12. The finite element grid used for the undrained analyses is shown in Figure 4.13. For an undrained strength of 17.1 TSM the bearing capacity is 87.9 TSM. The non-dilatant model predicts a bearing capacity of about 85 TSM. Run 31 is the result of the Tresca model which fails at a bearing capacity of 88 TSM. The only difference between Run 30 and Run 31 is that the non-dilatant model is the Tresca constitutive relations for small strains and the Tresca model is the Tresca constitutive relations for large strains. The two formulations produce similar results until yielding starts to occur. At loads

close to failure the large strain formulation produces a better solution for the stresses as evidenced by the close prediction of the failure load.

The large strain hyperbolic model produces good results for a footing on purely cohesive soil, Run 32 in Figure 4.12. The elastic constants input to each of the three models used to obtain the results in Figure 4.12 are the same; however, the hyperbolic model requires additional soil parameters which were chosen as reasonable approximations for Run 32. Consequently, for a given load the hyperbolic model produces more displacement than the non-dilatant and Tresca models and the failure load is less.

The spread of the yielded zone beneath a footing on undrained material is shown in Figure 4.14 for the large strain Tresca constitutive relation. Unlike a frictional material which develops a significant yielded zone at a low percent of the final failure load, the cohesive material does not begin to yield until almost half the final failure load has been applied. However, part of this behavior is due to the fact that the frictional material analyses were done using K_o initial conditions; whereas the undrained analyses were done with isotropic initial conditions.

Table 4.1 SUMMARY OF RETAINING WALL ANALYSES

Run	Model	Problem	Soil Parameters E	μ	c	ϕ	K_o	γ
1	Non-dilatant	Smooth Active Wall-Translation	30,000	0.3	0	30	.5	2.0
2	Non-dilatant	Smooth Passive Wall-Translation	30,000	0.3	0	30	.5	2.0
3	Non-dilatant	Rough Active Wall-Translation	30,000	0.3	0	30	.5	2.0
4	Non-dilatant	Rough Passive Wall-Translation	30,000	0.3	0	30	.5	2.0
5	Non-dilatant	Smooth Active Wall-Rotation	30,000	0.3	0	30	.5	2.0
6	Non-dilatant	Rough Active Wall-Rotation	30,000	0.3	0	30	.5	2.0
7	Non-dilatant	Rough Passive Wall-Rotation	30,000	0.3	0	30	.5	2.0
8	Dilatant	Smooth Active Wall-Translation	30,000	0.3	0	30	.5	2.0
9	Dilatant	Smooth Passive Wall-Translation	30,000	0.3	0	30	.5	2.0
10	Dilatant	Rough Passive Wall-Translation	30,000	0.3	0	30	.5	2.0
11	Strain Hardening	Smooth Passive Wall-Translation	30,000	0.3	0	30	.5	2.0

* Additional parameters required for strain hardening model.

$C_d = .05$ $D = 1.5$ $\beta = 0$

Table 4.2 COEFFICIENTS OF HORIZONTAL COMPONENT OF EARTH PRESSURE[1]

	RANKINE	COULOMB	SOKOLOVSKI	JANBU	BRINCH HANSEN	LOG SPIRAL	CAQUOT KERISEL
Passive	100%	298	195	205	180	185	218
Active	100%	77	80	73	81	80	--

1 From Morgenstern and Eisenstein (1970)

Table 4.3: SUMMARY OF BEARING CAPACITY ANALYSES

Run	Model	Problem	Soil Parameters E(TSM)	μ	c(TSM)	φ	K_o	γ(TSM)
21	Non-dilatant	Rigid Rough Footing	30,000	0.3	0	30	0.5	2.0
22	Non-dilatant	Rigid Rough Footing	30,000	0.3	0	30	0.5	2.0
23	Non-dilatant	Rigid Rough Footing	30,000	0.3	0	30	0.5	2.0
24	Non-dilatant	Rigid Rough Footing	30,000	0.3	0	30	0.5	2.0
25	Non-dilatant	Flexible Rough Footing	30,000	0.3	0	30	0.5	2.0
26	Dilatant	Rigid Rough Footing	30,000	0.3	0	30	0.5	2.0
27	Dilatant	Rigid Rough Footing	30,000	0.3	0	30	0.5	2.0
28	Dilatant	Rigid Rough Footing[1]	30,000	0.3	0	30	0.5	2.0
29	Strain Hardening	Rigid Rough Footing	30,000	0.3	0	30	0.5	2.0[2]
30	Non-dilatant	Flexible Rough Footing	30,000	0.2	17.1	0	1.0	0
31	Tresca	Flexible Rough Footing	30,000	0.2	17.1	0	1.0	0
32	Hyperbolic	Flexible Rough Footing	30,000	0.2	17.1	0	1.0	0[3]
33	Hyperbolic	Rigid Rough Footing	30,000	0.3	0	30	1.0	0[4]

[1]Free right boundary
[2]Additional parameters required - C_d=.05, D=1.5, β=0.
[3]Additional parameters required - n=1, R_f=.9, p_a=10.33 TSM
[4]Additional parameters required - n=.5, R_f=.95, p_a=10.33 TSM

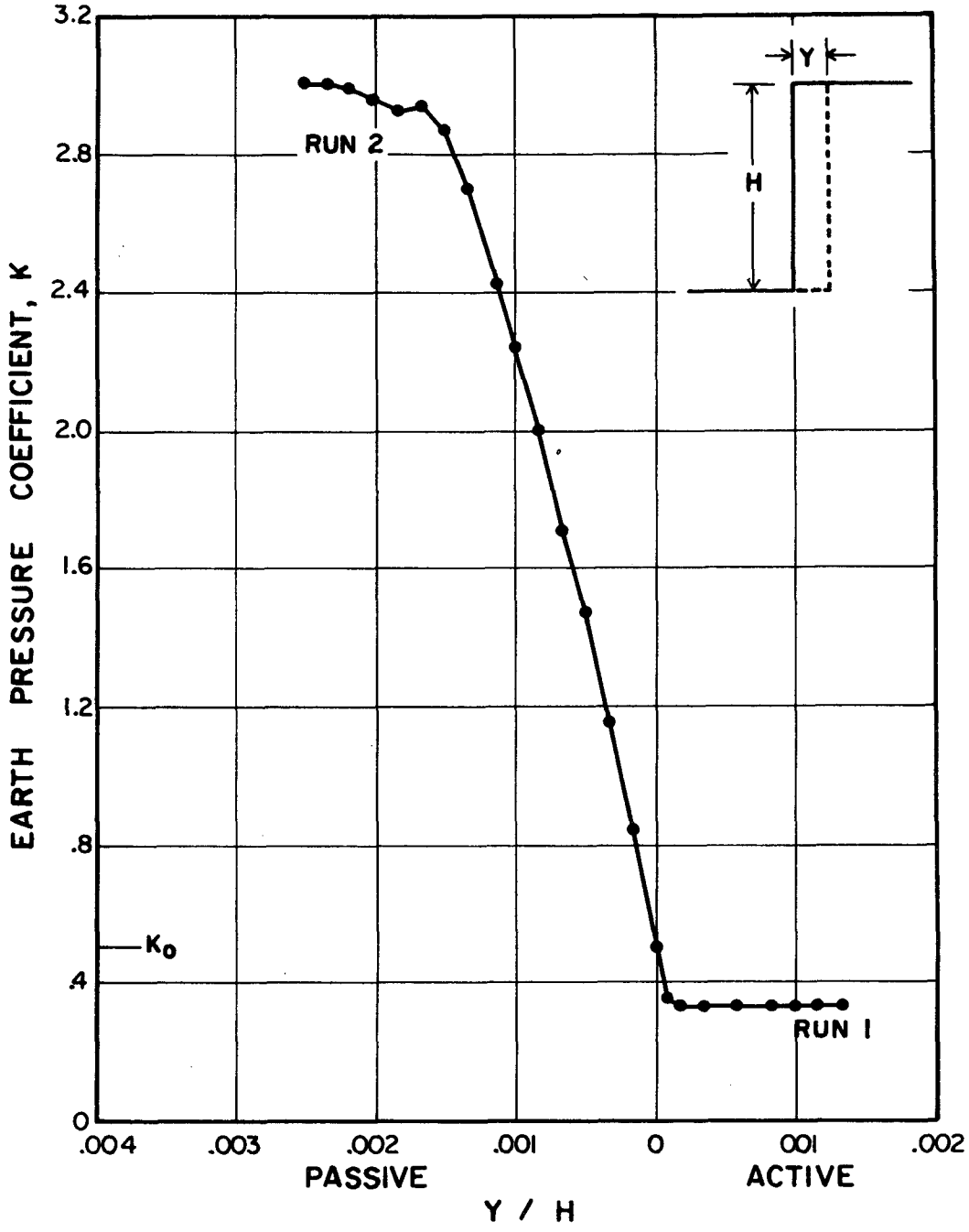

FIGURE 4.1 : SMOOTH RETAINING WALL AND NON-DILATANT MODEL

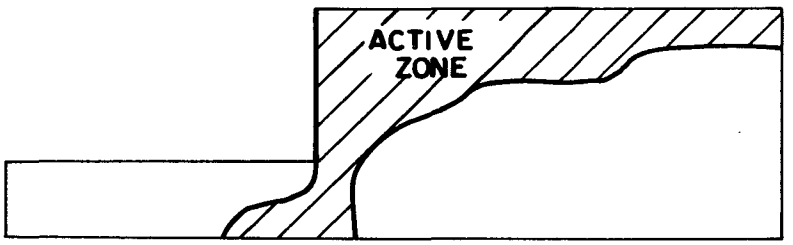

(a)

ACTIVE

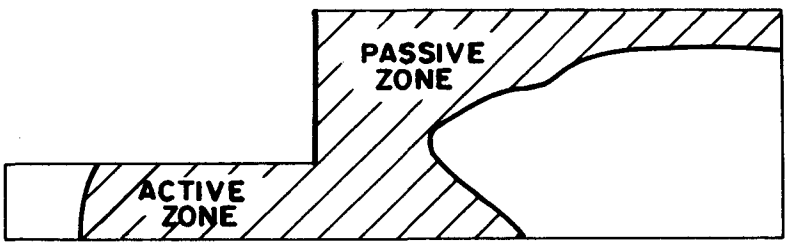

(b)

PASSIVE

FIGURE 4.2 : ACTIVE AND PASSIVE YIELDED ZONES

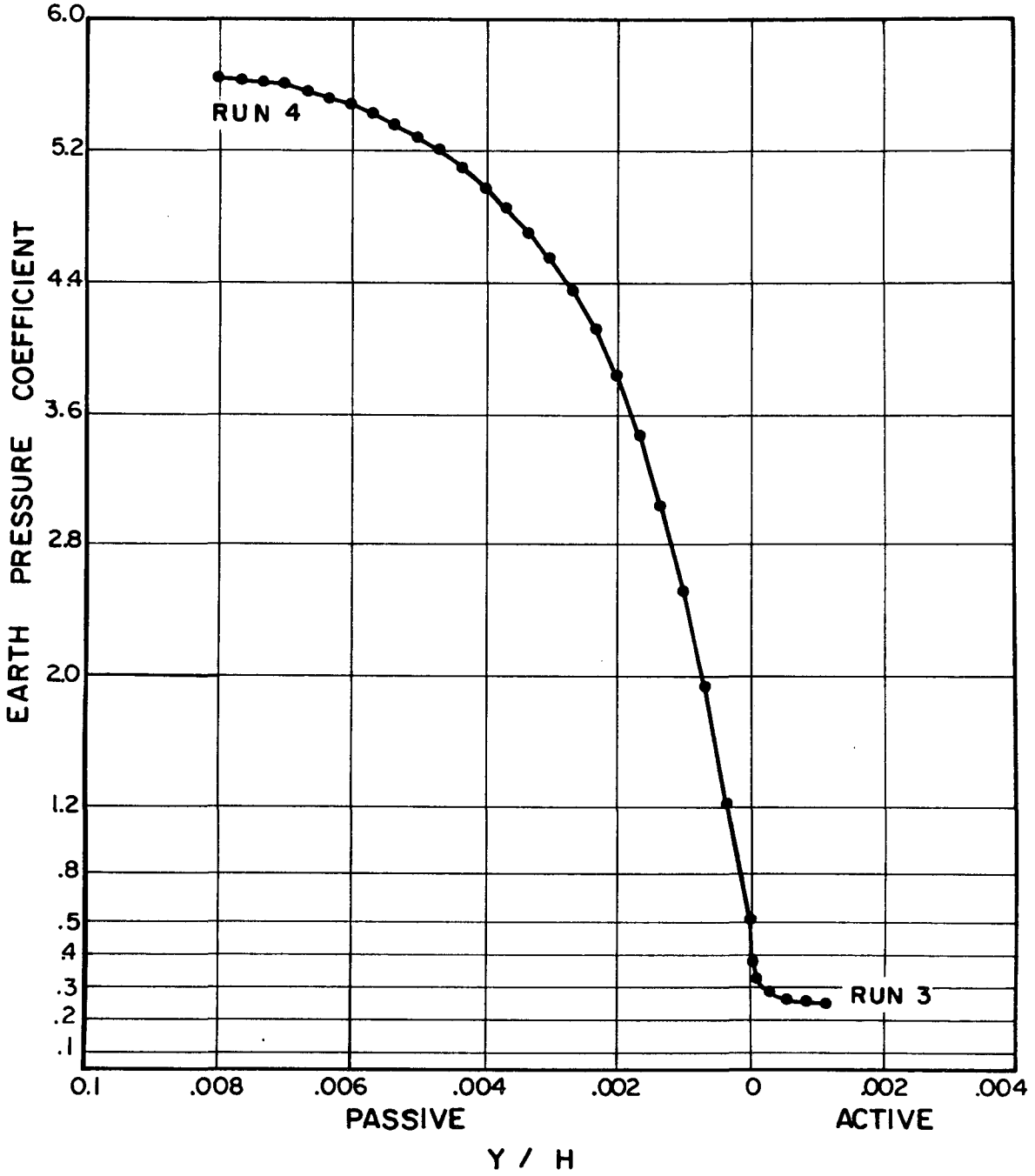

FIGURE 4.3 : ROUGH RETAINING WALL AND NONDILATANT MODEL

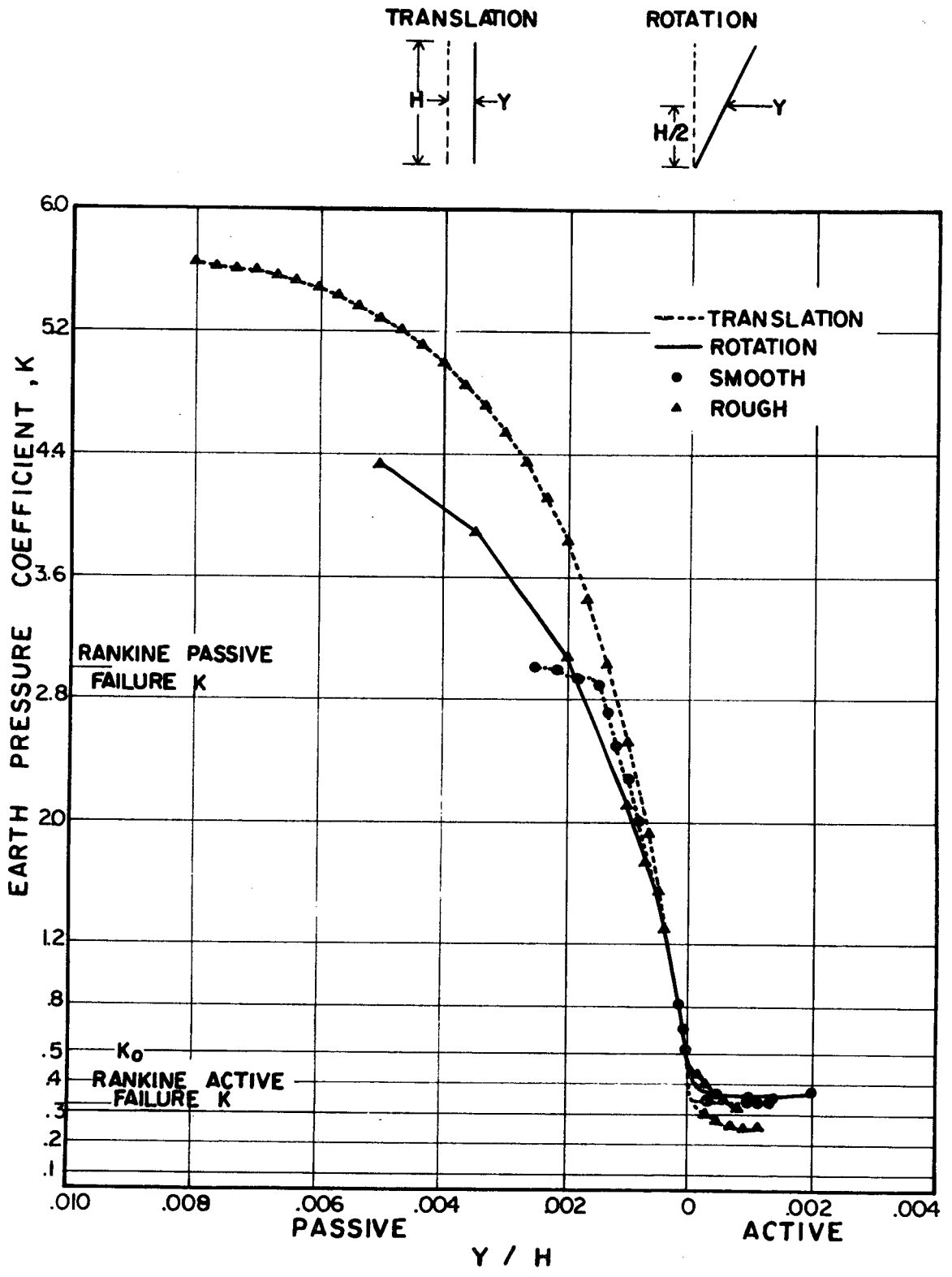

FIGURE 4.4: ROTATION VRS. TRANSLATION OF RETAINING WALL

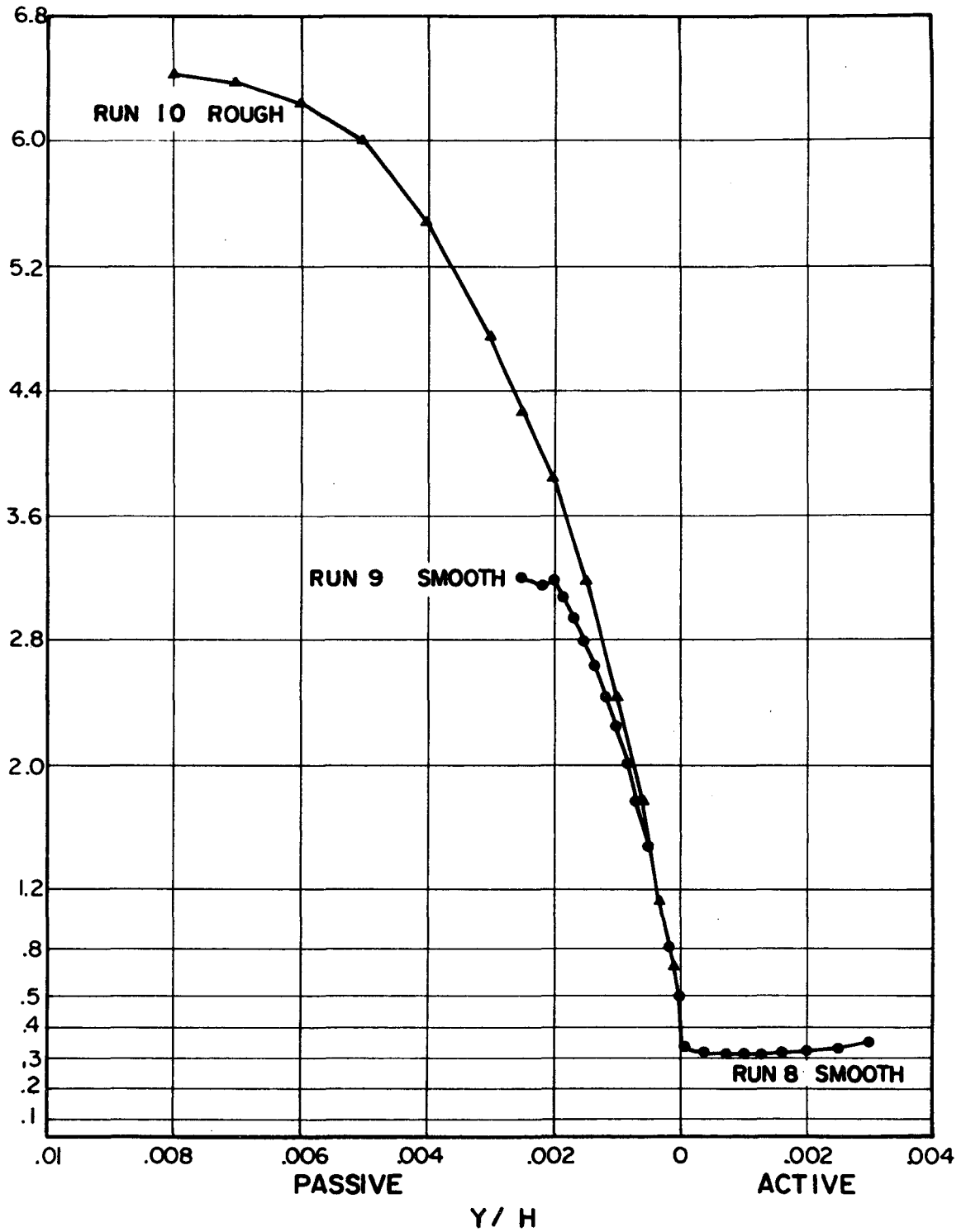

FIGURE 4.5 : TRANSLATION OF WALL WITH DILATANT MODEL

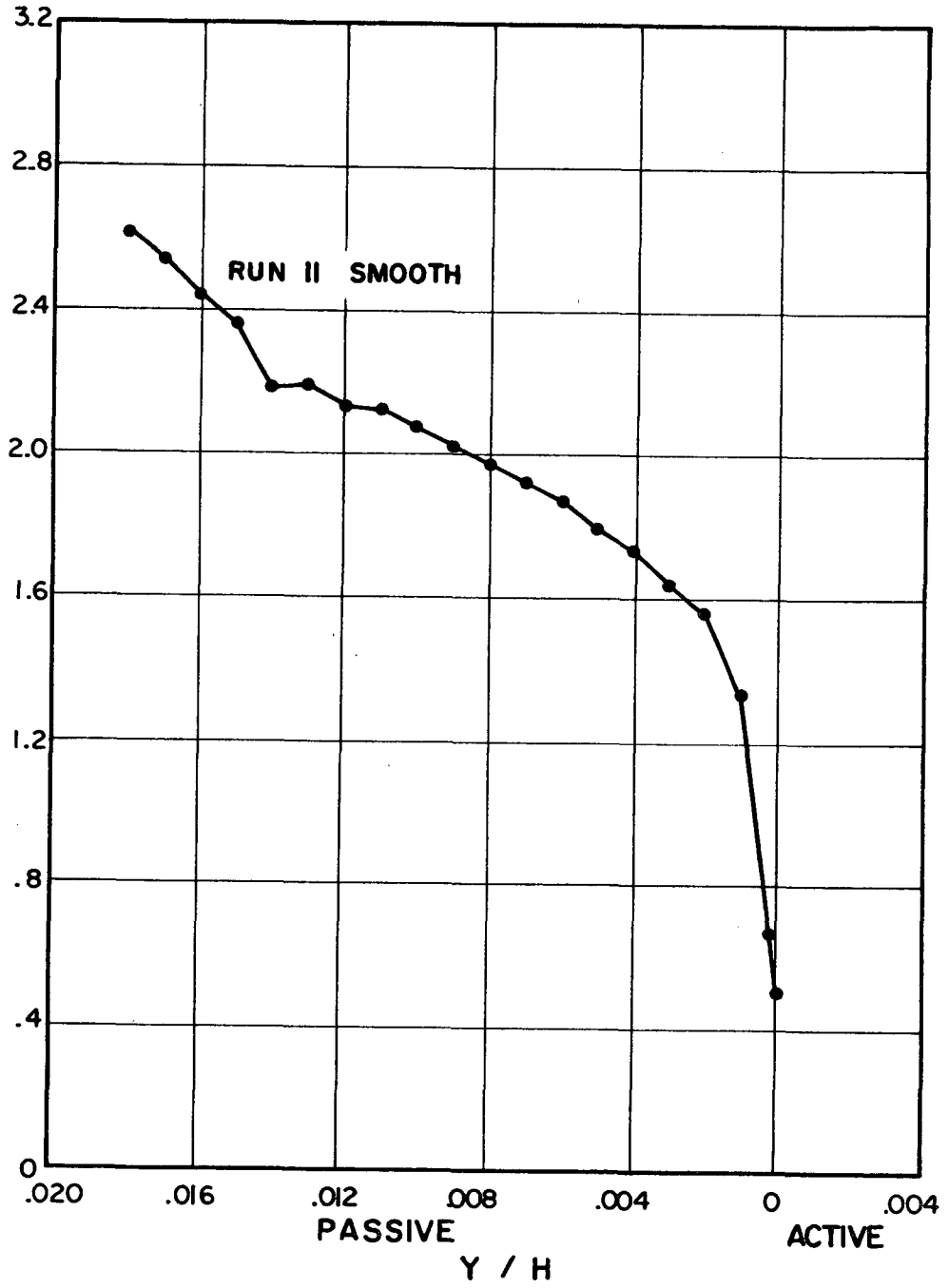

FIGURE 4.6: TRANSLATION OF WALL WITH STRAIN HARDENING MODEL

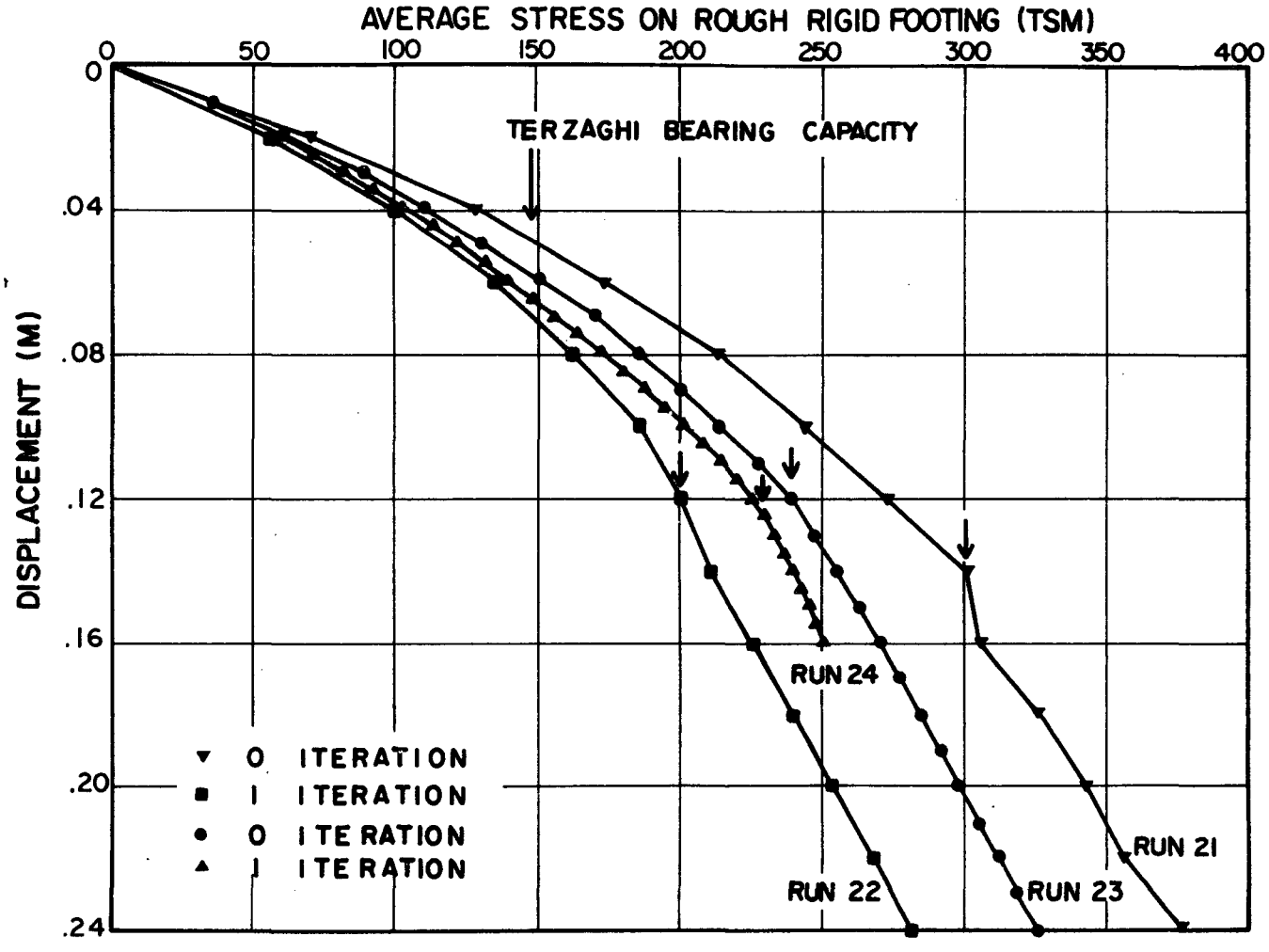

FIGURE 4.7 : SOLUTIONS FOR ROUGH RIGID FOOTING

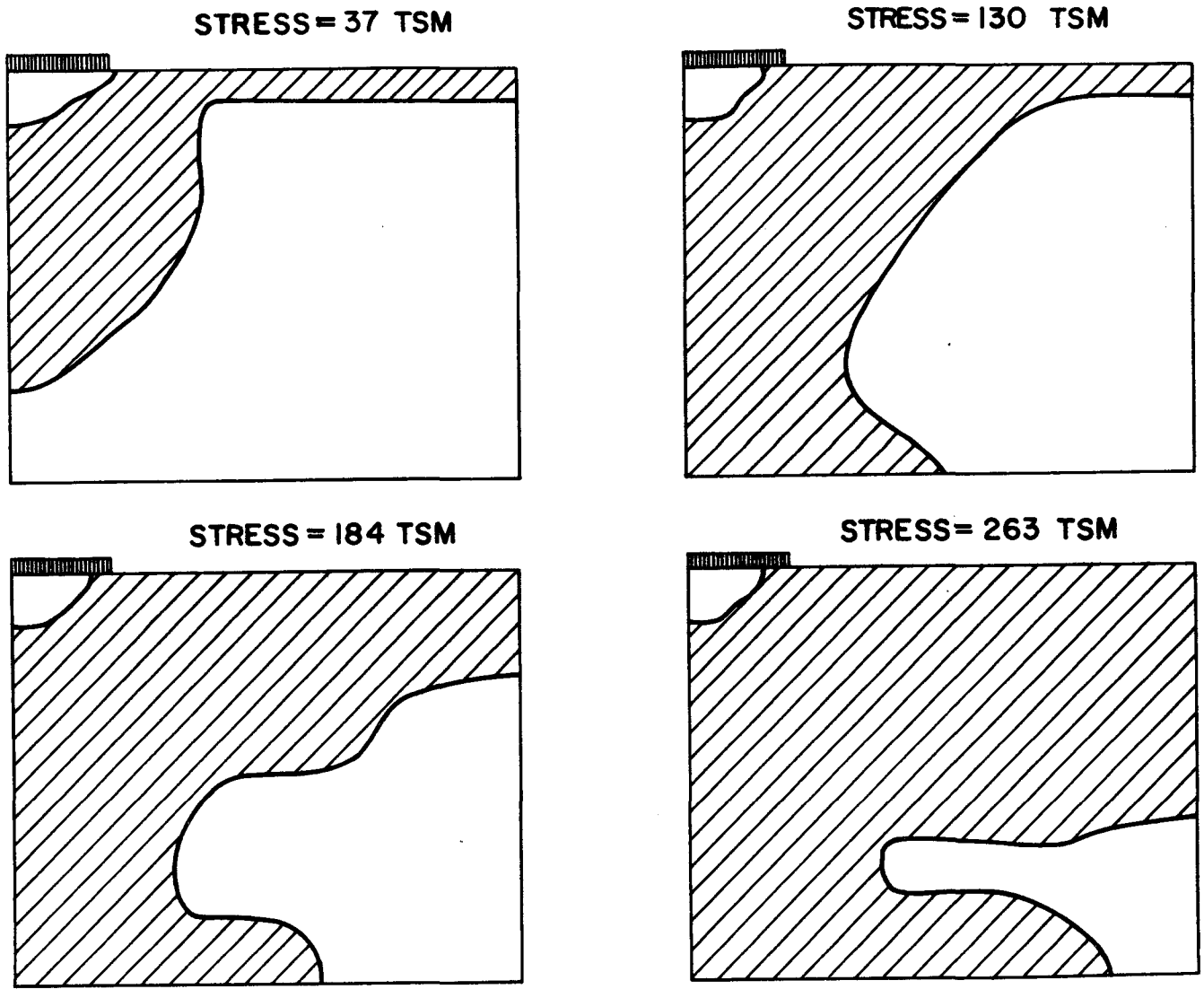

FIGURE 4.8 : SPREAD OF YIELDED ZONES IN FRICTIONAL MATERIAL

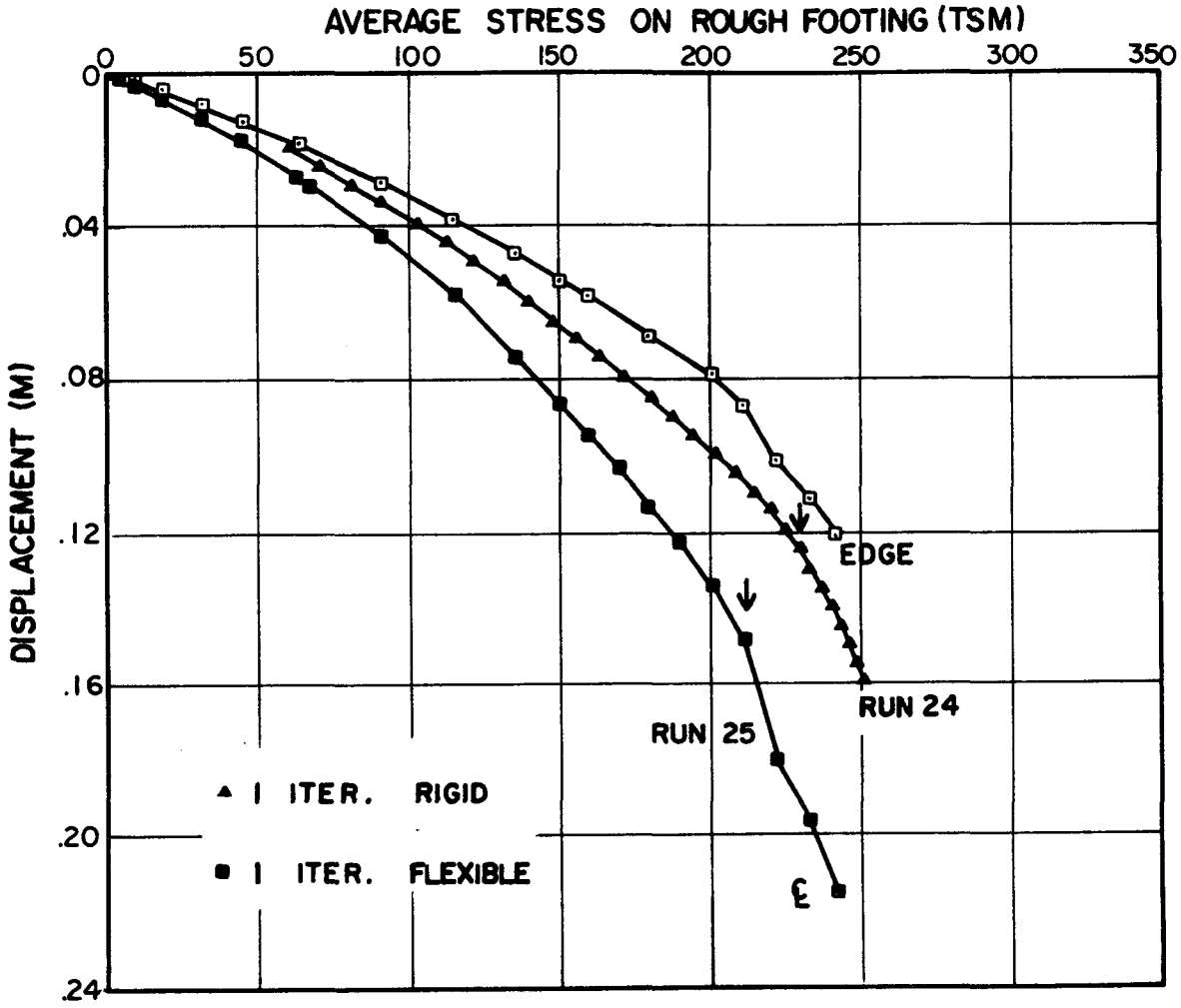

FIGURE 4.9: FLEXIBLE VRS RIGID FOOTING

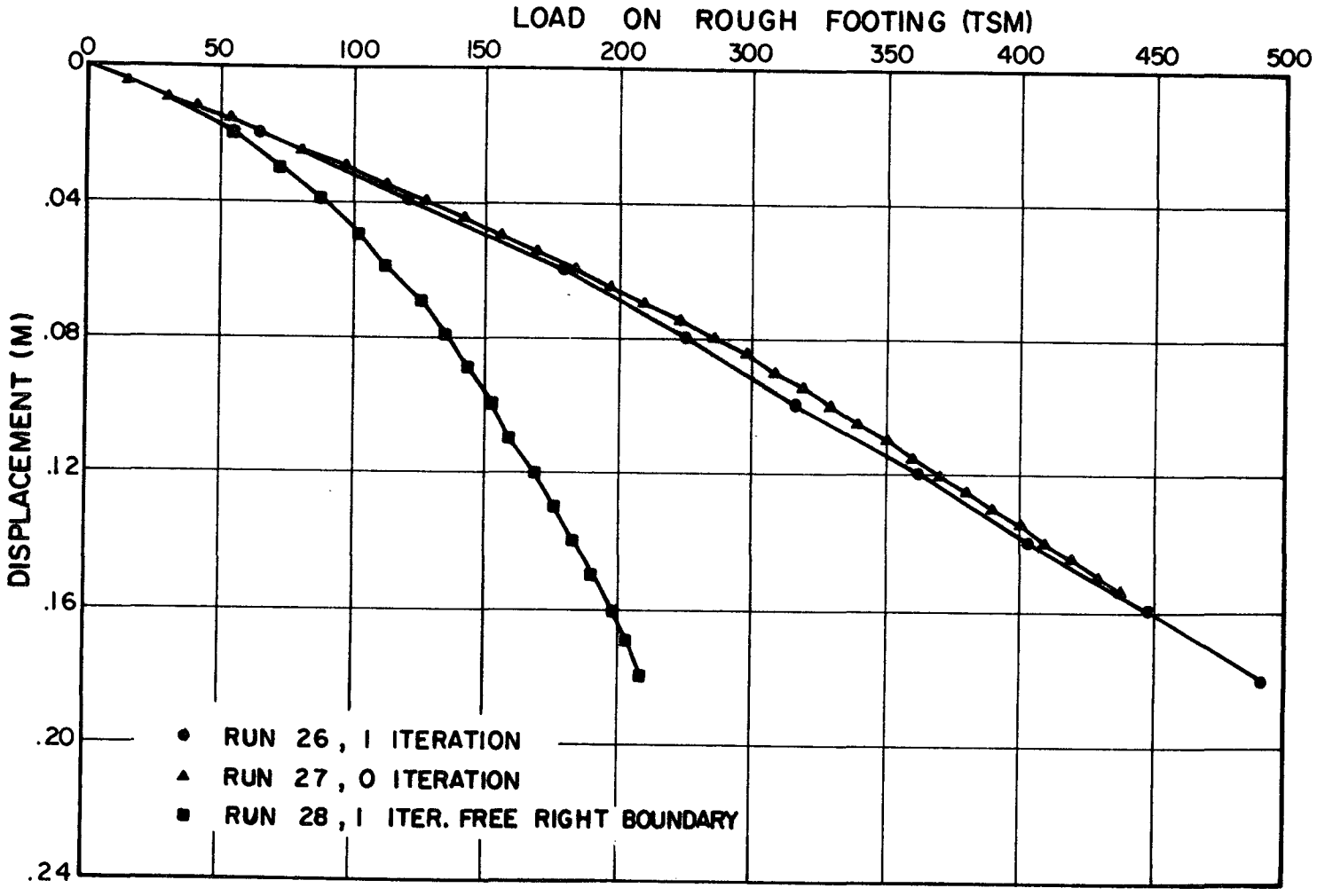

FIGURE 4.10 : RIGID FOOTING WITH DILATANT MODEL

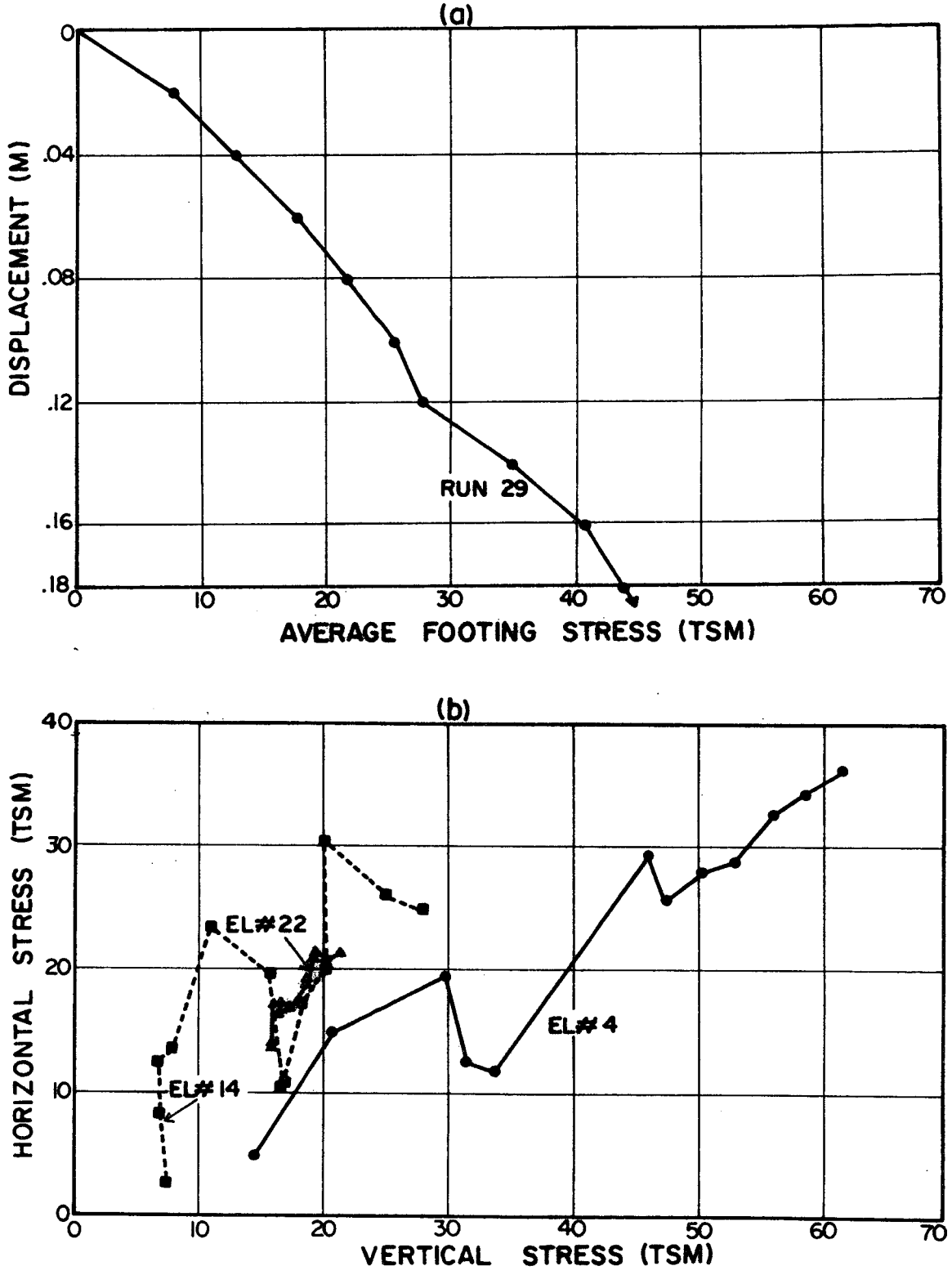

FIGURE 4.11: RIGID FOOTING WITH STRAIN HARDENING MODEL

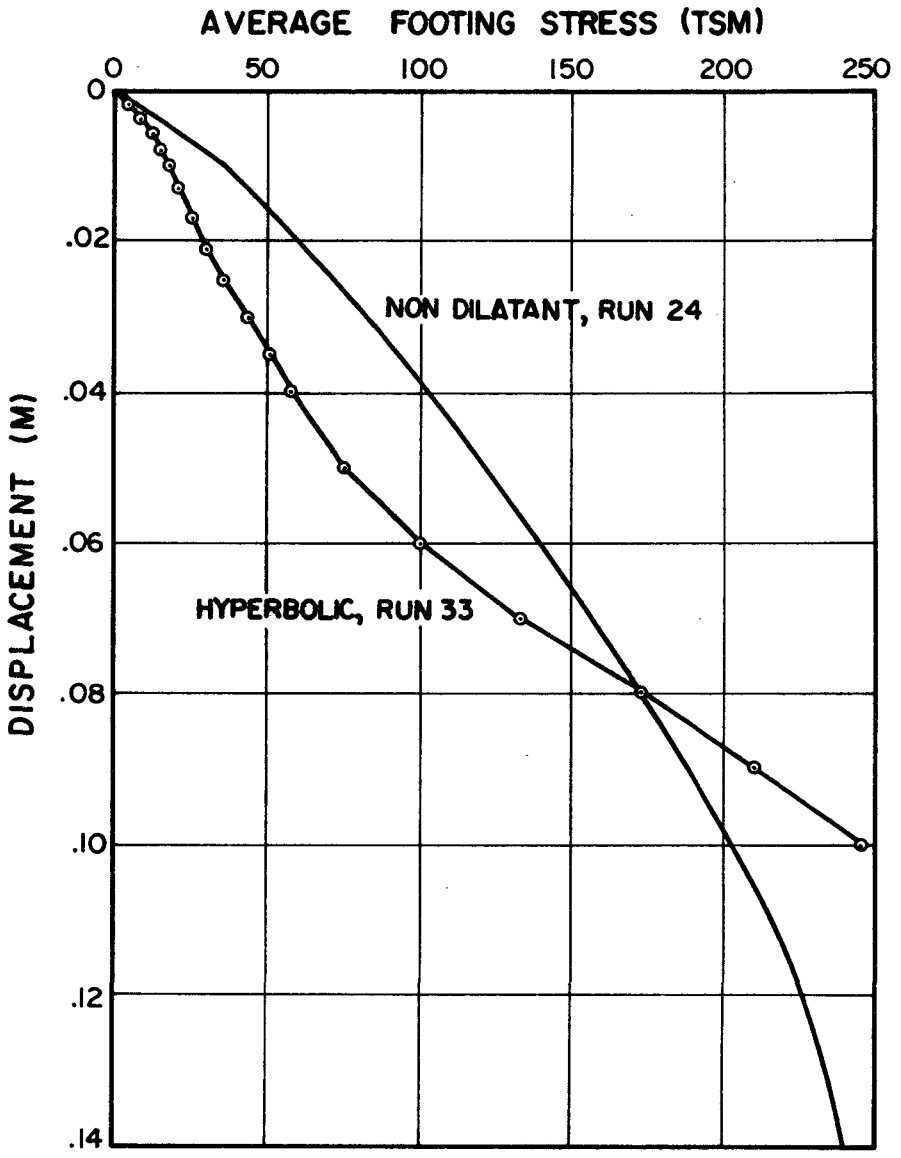

FIGURE 4.12 : HYPERBOLIC MODEL IN FRICTIONAL MATERIAL

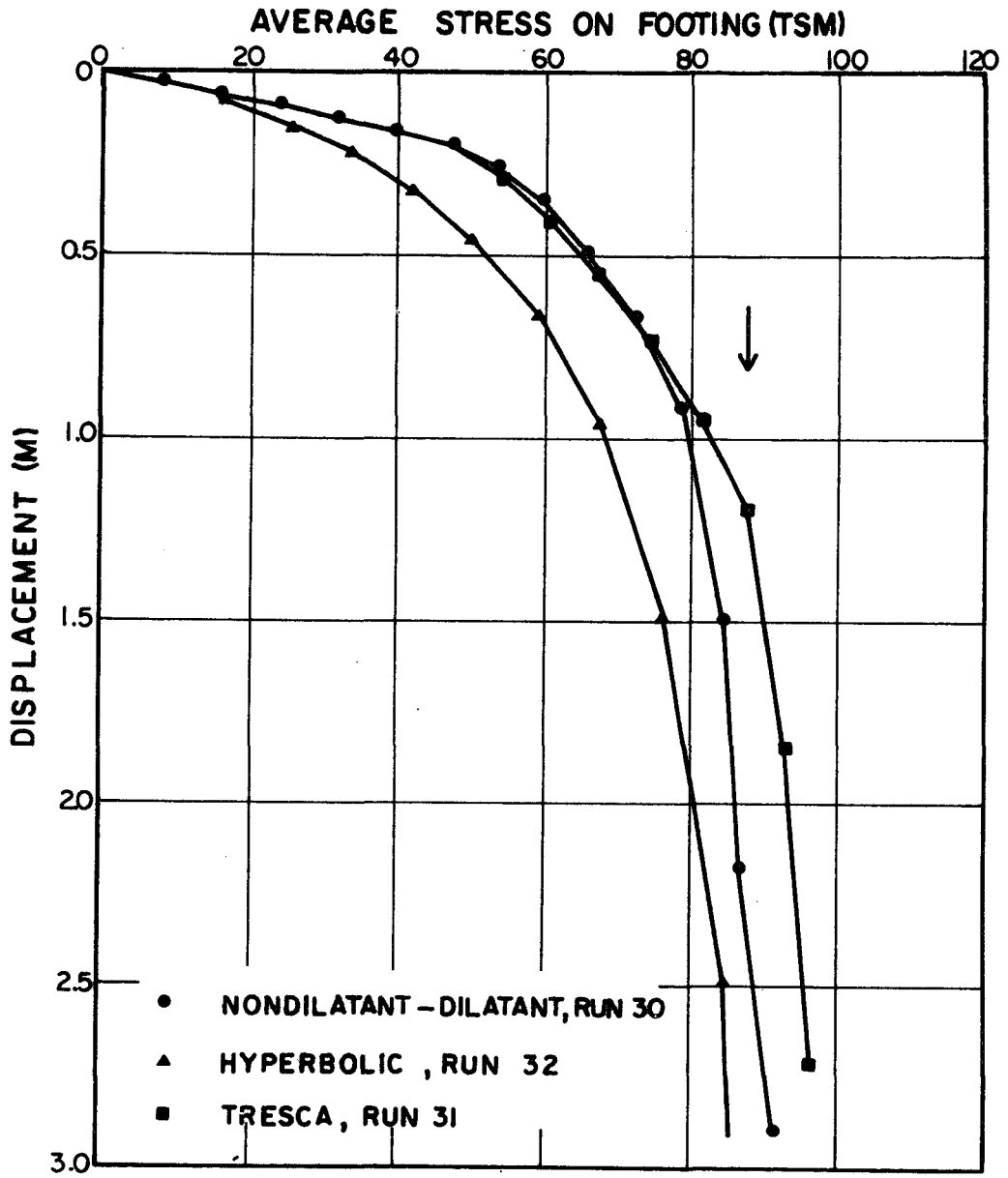

FIGURE 4.13: FLEXIBLE FOOTING ON COHESIVE SOIL

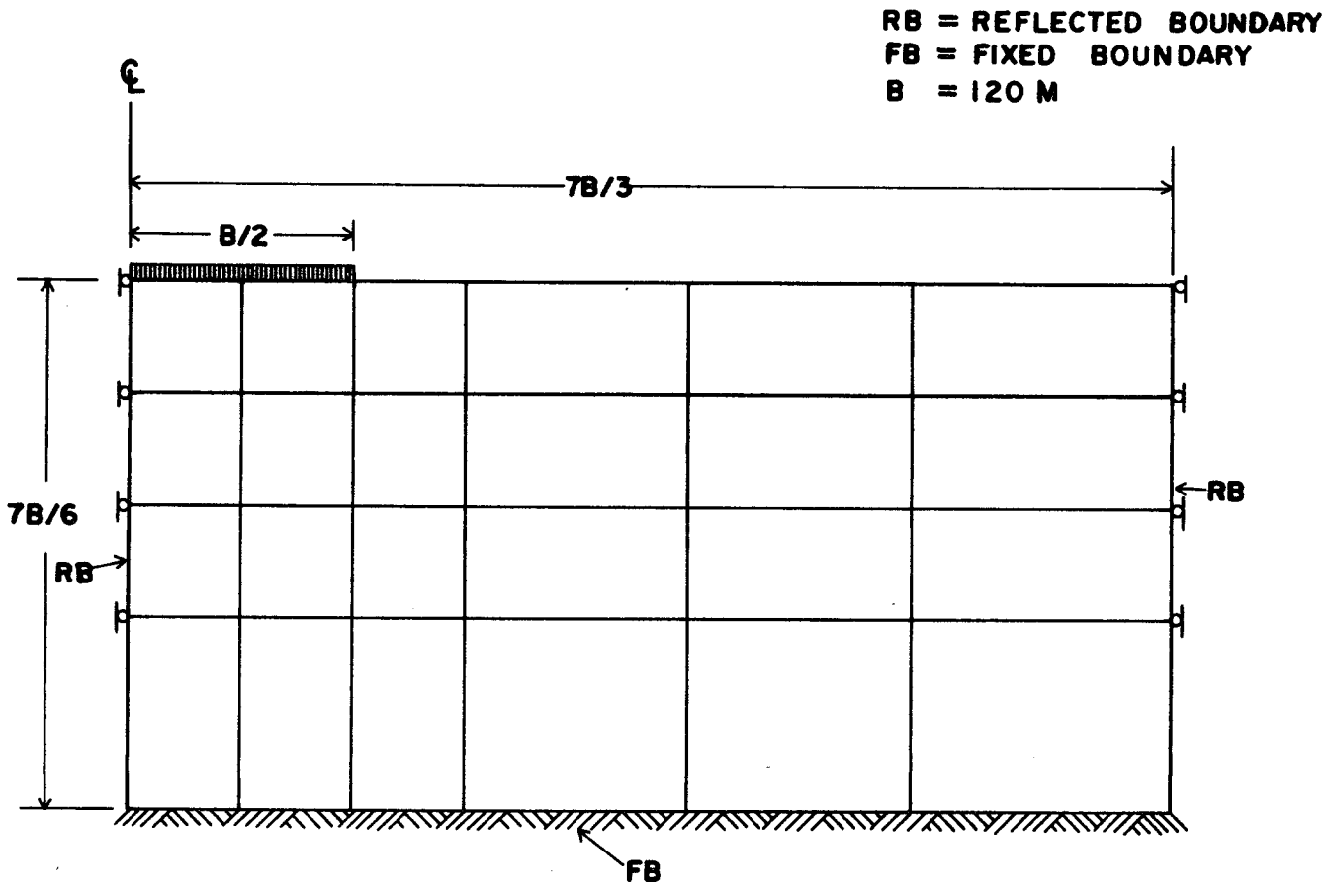

FIGURE 4.14 : GRID USED FOR UNDRAINED ANALYSES

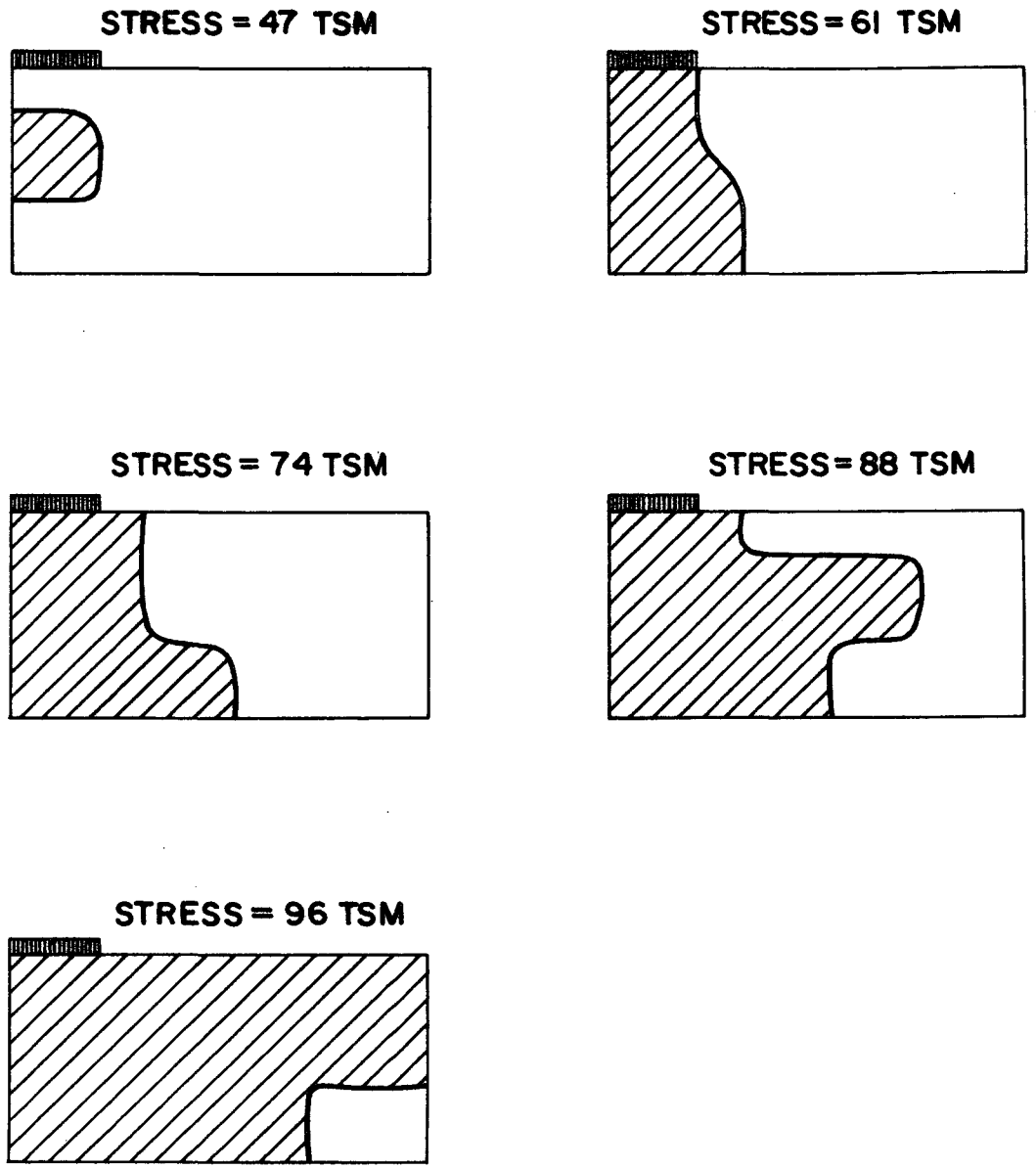

FIGURE 4.15: SPREAD OF PLASTIC ZONES IN LARGE STRAIN TRESCA MATERIAL, RUN 31

Chapter 5

CONCLUSIONS AND RECOMMENDATIONS

The behavior of finite element models employing five different constitutive relations to describe the stress-strain behavior of soils has been investigated by analyzing the load-deformation behavior of retaining walls and footings. The constitutive relations describe a strain hardening material, a dilatant material and a non-dilatant material using a small strain formulation and a Tresca elastic-perfectly plastic material and a material with a hyperbolic stress-strain relation using a large strain formulation. Hagmann (1971) developed the finite element programs for the small strain formulations and Molina (1971) developed those for the large strain formulations.

The effects of varying the finite element model were considered and several conclusions can be drawn:

1) For a given amount of computer time, smaller load increments provide a better solution for a non-linear material than a larger number of elements, provided there are enough elements to model the significant aspects of the problem.

2) For footing and retaining wall problems, there is a tendency for tension stresses to develop in surface elements. This behavior can be overcome by reducing the stiffness of tensile elements and changing their stresses to zero values.

3) For stress states which exceed the Mohr-Coulomb failure envelope, applying a correction which does not change the vertical stress produces good results.

4) Unless corrections are applied to the strain and nodal force computations to make them consistent with the corrected stresses which have exceeded the yield criteria, loads should be computed from element stresses rather than nodal forces.

Each of the constitutive relations were used to obtain solutions to footing and retaining wall problems. The following conclusions can be obtained:

1) Both the dilatant and non-dilatant models give results for the failure of retaining walls which are in good agreement with published analytical solutions.

2) The non-dilatant model gives a reasonable solution for the bearing capacity problem in a frictional material, while the dilatant model is too strong when the side boundary is fixed.

3) The strain hardening model needs an additional relation which describes the stress-strain behavior on the Mohr-Coulomb failure envelope.

4) The large strain hyperbolic model appears to be very sensitive to large values of Poisson's Ratio for frictional materials. More work is required to obtain the best way to formulate a hyperbolic stress-strain constitutive relation in a large strain analysis of frictional materials.

5) The non-dilatant, dilatant, hyperbolic and Tresca relations give good solutions for the undrained failure of footings. The large strain Tresca formulation improves the stress-strain behavior at stress levels close to failure.

In general the finite element method combined with an appropriate constitutive relation can predict the correct failure behavior of soil behind retaining walls. The bearing capacity problem for frictional soils is much more complex and good solutions are more difficult

if not impossible to obtain either analytically or by the finite element method.

Several recommendations for future research can be given:

1) An additional relation which describes the stress-strain behavior of stress states on the Mohr-Coulomb envelope should be added to the strain hardening model. Either the plastic relations of the non-dilatant model or a strain-softening constitutive relation seem appropriate.
2) The sensitivity of the large strain hyperbolic formulation to large values of Poisson's Ratio needs to be examined. A reformulation in terms of other elastic constants may be necessary to obtain the stress-strain behavior of frictional materials.
3) The non-dilatant model should be used to predict the results of field cases for the bearing capacity failure where the soil parameters are known to determine how appropriate its solutions are.
4) Each of the constitutive relations considered in this work fail to describe adequately behavior at stresses close to failure. Efforts to develop such a constitutive relation should be continued.

5) Finite element solutions are in general very expensive. Efforts should be made to apply these programs to common problems and by varying the important soil parameters generate parametric plots which can be useful in design by the engineering profession.

REFERENCES

Biot, M.A. (1965). Mechanics of Incremental Deformations, Wiley, New York.

Christian, J.T. (1966). "Two Dimensional Analysis of Stress and Strain in Soils", Report No. 3: Plane Strain Deformation Analysis of Soil, U.S. Army WES.

Clough, R.W. (1960). "The Finite Element Method in Plane Stress Analysis". Proc. 2nd ASCE Conf. on Electronic Computation, Pittsburg, Pennsylvania.

Clough, R.W. (1965). "The Finite Element Method in Structural Mechanics", Chap. 7 of Stress Analysis by Zienkiewicz, O.C. and G.S. Holister, John Wiley and Sons, pp. 85-119.

Clough, R.W. and J.L. Tocher (1965). "Finite Element Stiffness Matrices for Analysis of Plates in Bending", Proc. Conf. Matrix Methods in Structural Mechanics, Air Force Inst. of Technology, Wright Patterson Air Force Base, Ohio.

Coulomb, M. (1776). "Essai sur une application des règles de Maximis et Minimis à quelques problèmes de statique, relatifs a l'architecture", Mémoires de Mathématique et de Physique, Académie Royale des Sciences, Paris.

Drucker, D.C. and W. Prager (1952). "Soil Mechanics and Plastic Analysis of Limit Design", Quarterly of Applied Mathematics, Vol. 10, No. 2, pp. 157-165.

Drucker, D.C., R.E. Gibson, and D.J. Henkel (1957). "Soil Mechanics and Work-Hardening Theories of Plasticity", Transactions ASCE, Vol. 122, pp. 338-346.

Duncan, J.M. and C.Y. Chang (1970). "Non-linear Analysis of Stress and Strain in Soils", Proc., ASCE, JSMFE, Vol. 96, No. SM5, pp. 1639-1653.

Felippa, C.A. (1966). "Refined Finite Element Analysis of Linear and Non-linear Two-Dimensional Structures", Report to National Science Foundation, NSF Grant GK-75, University of California at Berkeley.

Gorbunov-Possadov, M.I. (1965). "Calculations for the Stability of a Sand Bed by a Solution Combining the Theories of Elasticity and Plasticity", Proc. Sixth Conf. Soil Mech. and Foun. Engr., Montreal, Vol. II, pp. 51-55.

Hagmann, A.J., J.T. Christian and D.J. D'Appolonia (1970). "Stress-Strain Models for Frictional Materials", M.I.T. Dept. of Civil Engineering Report R70-18.

Hagmann, A.J. (1971). "Prediction of Stress and Strain Under Drained Loading Conditions", M.I.T. Dept of Civil Engineering Report R71-3.

Hansen, J.B. (1953). Earth Pressure Calculation, Danish Tech. Press. Inst. of Danish Civil Engineers, Copenhagen.

Janbu, N. (1957). "Earth Pressure and Bearing Capacity Calculations by Generalized Procedure of Slices", Proc. 4th Int. Conf. Soil Mech. Foun. Engr., Vol. 2, pp. 207-212.

Kondner, R.L. (1963). "Hyperbolic Stress-Strain Response: Cohesive Soils", Proc., ASCE, JSMFD, Vol. 89, No. SM1, pp. 115-143.

Kondner, R.L. and J.S. Zelasko (1963). "A Hyperbolic Stress-Strain Formulation for Sands", Proc., 2nd Panamerican Conf. on Soil Mech. and Foun. Engr., Brizil, Vol. 1, pp. 289-324.

Kötter, F. (1903). "Die Bestimmung des Druckes an gekrümmten Gleitflächen, Sitzungsber. kgl. Preuss. Akad. der Wiss., Berlin.

Lundgren, H., and Mortensen, K. (1953). "Determination by Theory of Plasticity of Bearing Capacity of Continuous Footings on Sand", Proc., 3rd Int. Conf. on Soil Mech. and Foun. Engr., Zurich, Vol. 1, pp. 409-412.

Mises, R.V. (1928). "Mechanik der plastischen Formänderung der Kristallen", Z. angew. Math. Mech. 8, pp. 161-185.

Molina, R.F. (1971). "Finite Element Analysis of Large Strain in Soils", M.I.T. Dept. of Civil Engineering, Report R71-37.

Morgenstern, N.R. and Z. Eisenstein (1970). "Methods of Estimating Lateral Loads and Deformations", ASCE Spec. Conf. 'Lateral Stresses in the Ground and the Design of Earth-Retaining Structures', Cornell University.

Rankine, W.J.M. (1857). "On the Stability of Loose Earth", Trans. Royal Soc., London, Vol. 147.

Reddy, S.A. and R.J. Srinivasen (1970). "Bearing Capacity of Footings on Anisotropic Soils", Proc. ASCE, JSMFE, Vol. 96, No. SM6, p. 1978.

Roscoe, K.H., A.N. Schofield and C.P. Worth (1958). "On the Yielding of Soils", Geotechnique, Vol. 8, No. 1, pp. 25-53.

Roscoe, K.H., A.N. Schofield, and A. Thurairajah (1963). "Yielding of Soils in States Wetter than Critical", Geotechnique, Vol. 13, No. 3, pp. 211-240.

Roscoe, K.H., and J.B. Burland (1968). "On the Generalized Stress-Strain Behavior of 'Wet' Clay", from Engr. Plasticity, editors Heyman and Leckie, Cambridge Univ. Press.

Sokolovski, V.V. (1965). Statics of Granular Media, Trans. by J.K. Lusher, Pergamon Press.

Terzaghi, K. (1923). "Die Berechnung der Durchlässigkeitsziffer des Tones aus dem Verlauf der hydrodynamischen Spannungserscheinungen", Sitzber. Akad. Wiss, Wien, Abt. IIa, Vol.132.

Terzaghi, K. (1943). Theoretical Soil Mechanics, Wiley, New York.

Timoshenko, S. and J.N. Goodier (1951). Theory of Elasticity, McGraw-Hill, New York.

Wilson, E.L. (1965). "Structural Analysis of Axisymmetric Solids", AIAAJ, Vol. 3, No. 12, pp. 2269-2274.

Zienkiewicz, O.C. (1971). The Finite Element Method in Engineering Science, McGraw-Hill, London.

APPENDIX A

LIST OF SYMBOLS AND NOTATIONS

B	Bulk modulus; strip footing width
c	Cohesion intercept in the Mohr-Coulomb criterion
d	Cohesion intercept in p-q plane; $d=c\cdot\cos\phi$
D	Ratio of half-axes of elliptical yield surface
E	Young's Modulus
G	Shear modulus
H	Height of retaining wall
K	Coefficient of lateral earth pressure
K_o	Coefficient of lateral stress at rest
n	Rate exponent in hyperbolic model
N_γ	Bearing capacity factor
p	Value of $(\sigma_1+\sigma_3)/2$
p_a	Atmospheric pressure
q	Value of $(\sigma_1-\sigma_3)/2$
R_f	Failure ratio for hyperbolic model
S_u	Undrained strength of soil
α	Slope of failure envelope in p-q plane; $\tan\alpha = \sin\phi$
β	Frictional coefficient from Mohr-Coulomb failure criterion in 3-dim. space for strain hardening model
γ	Unit weight of soil
ϕ	Friction angle in Mohr-Coulomb criterion

μ	Poisson's ratio
σ_1	Major principal stress
σ_3	Minor principal stress
$\sigma_{xx}, (\sigma_{zz})$	Normal stresses in horizontal (vertical) direction
τ_{xz}	Shear stress in x,z directions in plane denotes modified value of stress

APPENDIX B

ADJUSTMENT OF STRESSES TO MOHR-COULOMB YIELD SURFACE

The Mohr-Coulomb line represents the maximum stress state an element may have. Due to the incremental nature of applying loads, element stress states may exceed the Mohr-Coulomb yield surface during a load increment. Since no state of stress may exceed the failure envelope, the stresses in these elements must be corrected. The three procedures developed are derived below. Table B.1 gives an example of the corrected stresses for each procedure.

B.1 Correction With Constant P, Subroutine MOCO1

Figure B.1 shows a computed stress state which exceeds the Mohr-Coulomb failure line. The failure line requires that for yielded elements

$$q' = d - p' \cdot \tan\alpha \qquad \text{(B-1)}$$

Primes (') are used to denote corrected stress values and symbols are defined in Appendix A. Correcting with constant p

$$\begin{aligned} p' &= p \\ q' &= d - p \cdot \tan\alpha \end{aligned} \qquad \text{(B-2)}$$

Let

$$a = q'/q$$

$$b = a \left(\frac{\sigma_{xx}-\sigma_{zz}}{2}\right) \tag{B-3}$$

Then it follows that

$$\begin{aligned} p' &= p \\ q' &= d - p\cdot\tan\alpha \\ \sigma_1' &= p + q' \\ \sigma_3' &= p - q' \\ \sigma_{xx}' &= p + b \\ \sigma_{zz}' &= p - b \\ \tau_{xz}' &= a\cdot\tau_{xz} \end{aligned} \tag{B-4}$$

This method reduces the radius of the Mohr's circle until a stress state compatible with the yield surface is reached. No rotation of principal planes occurs due to the correction.

B.2 Correction Perpendicular to Mohr-Coulomb Yield Surface, Subroutine MOCO2

Figure B.2 illustrates this procedure where both p and q are corrected. From geometry considerations we obtain

$$\frac{q - q'}{p - p'} = \cot\alpha \tag{B-5}$$

Combining Eqs. (B-5) and (B-1) and solving for p' and q'

$$p' = \frac{(d-q)\tan\alpha + p}{1 + \tan^2\alpha} \qquad \text{(B-6)}$$

$$q' = d - p' \cdot \tan\alpha$$

To solve for the corrected stresses we require that there be no rotation of principal planes induced by the correction technique, or

$$a = \frac{q'}{q} = \frac{\tau'_{xz}}{\tau_{xz}} \qquad \text{(B-7)}$$

Let

$$b = \frac{p'}{p} \qquad \text{(B-8)}$$

and we obtain

$$\begin{aligned}
\sigma_1' &= p' + q' \\
\sigma_3' &= p' - q' \\
\sigma_{xx}' &= \left(\frac{a+b}{2}\right)\sigma_{xx} + \left(\frac{b-a}{2}\right)\sigma_{zz} \\
\sigma_{zz}' &= \left(\frac{a+b}{2}\right)\sigma_{zz} + \left(\frac{b-a}{2}\right)\sigma_{xx} \\
\tau_{xz}' &= a\,\tau_{xz}
\end{aligned} \qquad \text{(B-9)}$$

where p' and q' are obtained from Eq. (B-6).

B.3 Correction Maintaining Vertical Stress Constant, Subroutine MOCO3

This correction procedure requires that stress states over the Mohr-Coulomb line be corrected without changing the vertical stress, σ_{zz}. Again we require that the correction does not produce rotation of principal planes.

$$a = \frac{q'}{q} = \frac{\tau_{xz}'}{\tau_{xz}} \tag{B-3}$$

Combining Eq. (B-3) with

$$q = \left[\left(\frac{\sigma_{zz}-\sigma_{xx}}{2}\right)^2 + \tau_{xz}^2\right]^{\frac{1}{2}}$$

and requiring that $\sigma_{zz}' = \sigma_{zz}$ we obtain

$$\left(\frac{\sigma_{zz}-\sigma_{xx}'}{2}\right)^2 + \tau_{xz}^2 = a^2\left[\left(\frac{\sigma_{zz}-\sigma_{xx}}{2}\right)^2 + \tau_{xz}^2\right] \tag{B-10}$$

The failure law may be written as

$$\left[\left(\frac{\sigma_{zz}-\sigma_{xx}'}{2}\right)^2 + \tau_{xz}'^2\right]^{\frac{1}{2}} = d - \left(\frac{\sigma_{zz}+\sigma_{xx}'}{2}\right)\tan\alpha \tag{B-11}$$

Equations (B-3), (B-10) and (B-11) are three equations with the unknowns τ_{xz}', σ_{xx}' and a. Solving these equations

we obtain

$$a = \frac{\sigma_{zz} \tan\alpha - d}{\frac{\tan\alpha}{2}(\sigma_{zz}-\sigma_{xx}) - q}$$

$$q' = a\, q$$

$$p' = \frac{d - q'}{\tan\alpha} \qquad \text{(B-12)}$$

$$\sigma_1' = p' + q'$$

$$\sigma_3' = p' - q'$$

$$\sigma_{xx}' = \frac{2}{\tan\alpha}(d - aq) - \sigma_{zz}$$

$$\sigma_{zz}' = \sigma_{zz}$$

$$\tau_{xz}' = a \cdot \tau_{xz}$$

This procedure is illustrated in Figure B.3.

Table B-1 EXAMPLE OF STRESS CORRECTION FOR THREE PROCEDURES

	UNCORRECTED STRESSES	CORRECTED STRESSES		
	ϕ=30° d=10	MOCO 1	MOCO 2	MOCO 3
p	-40	-40.00	-42.00	-42.22
q	35	30.00	31.0	31.11
σ_1	- 5	-10.00	-11.00	-11.11
σ_3	-75	-80.00	-73.00	-73.33
σ_{xx}	-20	-22.85	-24.29	-24.44
σ_{zz}	-60	-57.14	-59.71	-60.00
τ_{xz}	28.72	24.62	25.44	25.53

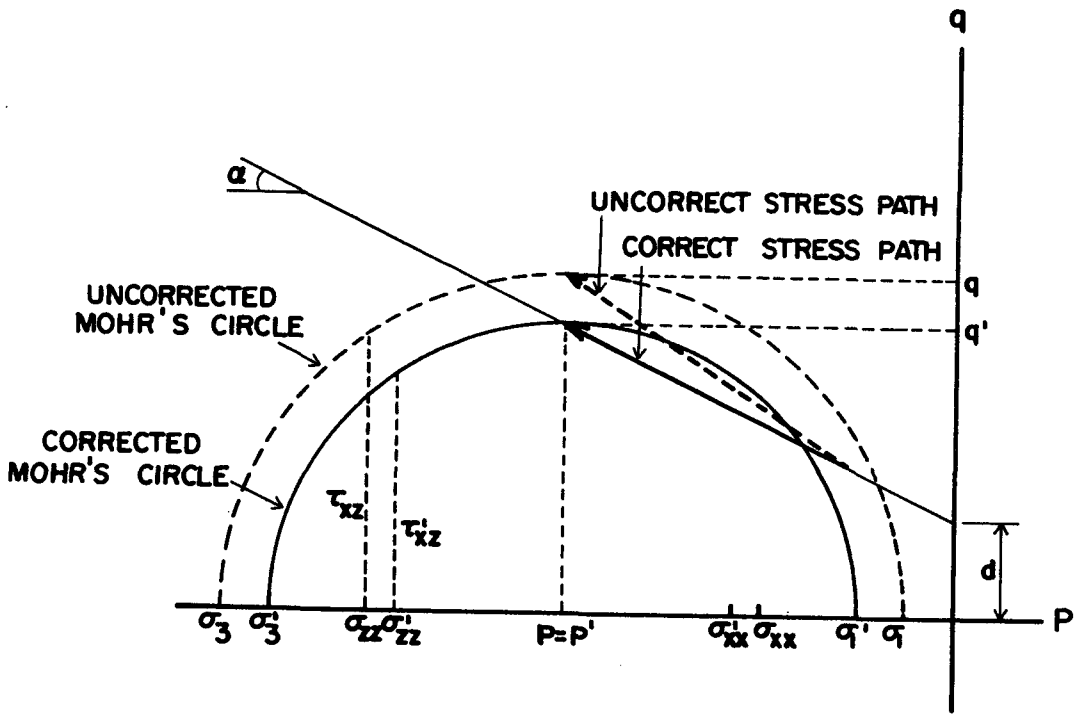

FIGURE B-1 : CORRECTION SCHEME WITH CONSTANT P

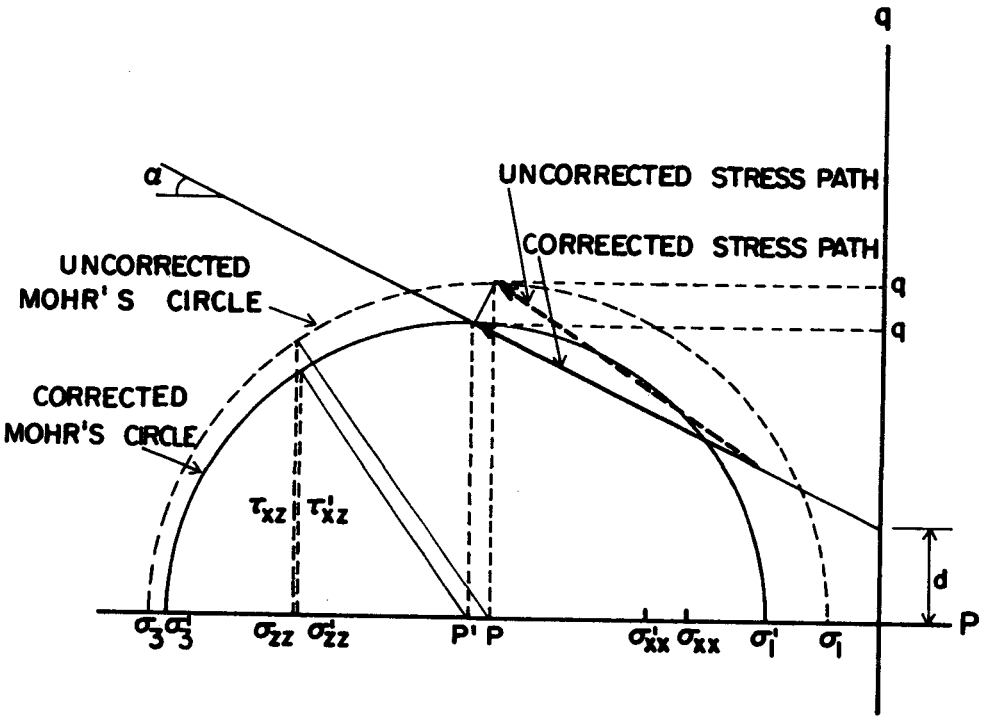

FIGURE B-2 : CORRECTION SCHEME WITH CORRECTION PERPENDICULAR TO MOHR-COULOMB LINE

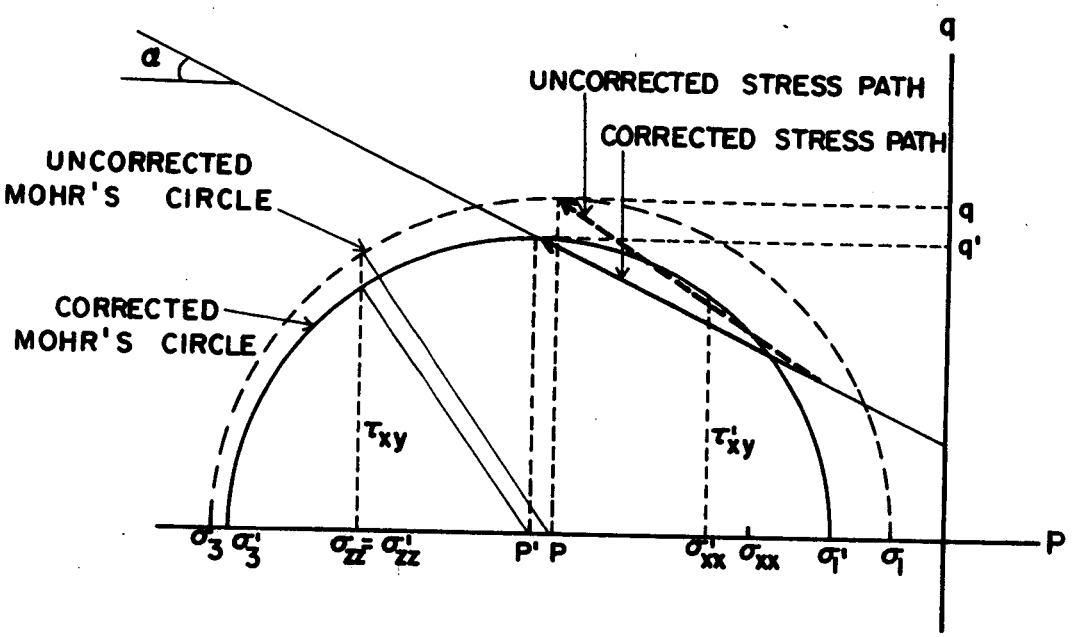

FIGURE B-3 : CORRECTION SCHEME WITH VERTICAL STRESS KEPT CONSTANT